Utrecht University
MSc Thesis

Paleointensity during the Laschamp and Blake geomagnetic excursions

Roy Lagerburg

January 31, 2013

Supervisor: L.V. de Groot, MSc

Abstract

Full vector information of the Earth's magnetic field on a geological time scale is essential to put constraints on geodynamo models. Excursions of the geomagnetic field show deviating directions and a strong decrease in intensity and they are thought to be caused by the same geodynamo processes as reversals. In this study we attempt to assess the properties of the paleofield during the Laschamp and Blake excursions by investigating 15 lava flows (28.6 - 154.9 ka) from Mount Etna on Sicily. Directions of the magnetization are obtained and the paleointensity is acquired by three different absolute methods (Thellier-Thellier, the original multispecimen protocol, and the domain state corrected multispecimen protocol) and one relative method (pseudo-Thellier).

Five sites were selected based on the preliminary measurements and yielded technically good results with all paleointensity methods. The Thellier-Thellier method yielded the highest paleointensity for these sites, which are taken as an upper bound. The MSP-DB method produced lower values that are taken as a lower bound for the paleointensity. Results of the MSP-DSC method were not reliable as they were clearly affected by alteration during subsequent heating steps. The calibration formula of the pseudo-Thellier method seemed not applicable to these specimens. A new calibration based on one of the absolute methods, however, could not be made. Resulting paleointensities range from 30.9 µT to 122.3 µT and could not be correlated to either the Laschamp or the Blake excursion. Two other sites might be related to the Laschamp excursion based on the age and direction, but a paleointensity could not be obtained.

CONTENTS

List of abbreviations

AF	Alternating field
ARM(-test)	Anhysteretic remanent magnetization (test)
CI	Confidence interval
DC	Direct current
IGRF	International Geomagnetic Reference Field
INGV	(Italian) National Institute of Geophysics and Volcanology
IZZI	In-field zero-field, zero-field in-field protocol
MD	Multi-domain
MSP	Multispecimen protocol
MSP-DB	Multispecimen protocol (Dekkers-Böhnel)
MSP-DSC	Domain state corrected multispecimen protocol
NRM	Natural remanent magnetization
PI	Paleointensity
PSD	Pseudo-single-domain
pTh(-slope)	Pseudo-Thellier (slope)
pTRM	Partial thermoremanent magnetization
SD	Single-domain
SQUID	Superconducting quantum interference device
TRM	Thermoremanent magnetization
UTM	Universal Transverse Mercator coordinate system
VGP	Virtual geomagnetic pole
WGS84	World Geodetic System 1984

1. Introduction

Knowledge of the Earth's magnetic field is important in different fields of research such as cosmic radiation, magnetostratigraphy, and geodynamo modeling. Full vector information of the geomagnetic field on a geological time scale could put essential constraints on models and results from these fields of research. The geomagnetic field is known to flip polarity regularly in the past (Gubbins, 1999; Valet, 2003), a phenomenon that is present in recent geodynamo models (Driscoll and Olson, 2009). During reversals, the intensity of the geomagnetic field is thought to decrease strongly (Valet, 2003), as a result of which more cosmic radiation could penetrate to the Earth's surface (Dekkers and Böhnel, 2006).

Excursions of the geomagnetic field are often associated with the same geodynamo processes as full reversals of the field (Gubbins, 1999). It is presumed that excursions are events in which the geomagnetic field reverses in the liquid outer core but not in the solid inner core, as is the case for reversals (Hollerbach and Jones, 1993; Gubbins, 1999). Therefore, understanding the behavior of the Earth's magnetic field during excursions is very important. Geomagnetic excursions are periods lasting only a few thousands of years during which the Earth's magnetic field shows strongly decreased intensities of 4 - 20 μT (Ferk and Leonhardt, 2009; Singer et al., 2009) and very deviating directions, often close to fully reversed field directions. The directional behavior of the paleofield (declination and inclination) can readily be assessed. However, determining the third component of the full vector description of the field, the paleointensity, is a bigger challenge (Valet, 2003; Biggin et al., 2007; Dunlop, 2011).

The most recent excursions that are globally observed are the Laschamp excursion, occurring 40.70 ± 0.95 ka (Roperch et al., 1988; Chauvin et al., 1989; Guillou et al., 2004; Ferk and Leonhardt, 2009; Singer et al., 2009; Vérard et al., 2012), and the Blake excursion, occurring 114.47 - 119.97 ka (Tric et al., 1991; Fang et al., 1997). This study attempts to further assess the properties of the paleofield during these excursions. For this purpose, lava flows from Mount Etna on Sicily potentially provide ideal sampling. Recent flows produced by Mount Etna have extensively been used for testing paleointensity methods (e.g. Biggin et al., 2007; de Groot, Dekkers, et al., 2012; de Groot et al., under revision) and recently a large amount of lava flows have been dated in the interesting time interval for the Laschamp and Blake excursion (De Beni et al., 2011; Del Carlo et al., 2012).

To account for the difficulties that are encountered in determining the paleointensity, different methods are used in this study. In the classical Thellier-Thellier method (Thellier and Thellier, 1959) the natural remanent magnetization (NRM) of a sample is progressively replaced by a partial thermal remanent magnetization (pTRM) at successively higher temperatures to obtain an absolute paleointensity. Improvements have been made to the method to increase the quality and reliability of the obtained results (Coe, 1967; Aitken et al., 1988; Riisager and Riisager, 2001), which are combined in the IZZI protocol that is used in this study (Tauxe and Staudigel, 2004; Yu et al., 2004). The original multispecimen method (MSP-DB, Dekkers and Böhnel, 2006) heats sister specimens only once to different field strengths to avoid any alteration or difference in magnetic history. This protocol was extended to the MSP-DSC (domain state corrected, Fabian and Leonhardt, 2010) to correct for the magnetic domain state and implement an alteration check. Both MSP protocols are absolute paleointensity methods and can be compared to the Thellier-Thellier method. Lastly, the pseudo-Thellier method is used, which uses alternating field (AF) demagnetization and anhysteretic remanent magnetization (ARM) acquisition to yield a relative measure of the paleointensity (De Groot, Biggin, et al., 2012).

2. Geological setting and sampling

Mount Etna is a basaltic composite stratovolcano of 3328 m height on the east coast of Sicily, Italy (Branca et al., 2011). The volcano is located between the Gela-Catania foredeep and the Hyblean foreland. The complex structural setting below Mount Etna originated in the Neogene during the convergence of the African and Eurasian plates.

Mount Etna is one of the most active volcanoes in the world, while located in a densely inhabited area. It has been continuously active since the first historical reports 2,700 years ago with eruptions from its summit craters and rather frequent lava flows from fissures on the flanks. Volcanic activity is thought to first started around 500 ka with submarine volcanics near the east coast of Sicily (De Beni et al., 2011). From then on, volcanic activity shifted in a westward direction to the central portion of the present edifice, with almost continuous activity over the last 150 ka.

For this research in general sampling sites were chosen from De Beni et al. (2011), who determined the age of forty sites by $^{40}Ar/^{39}Ar$ isotopic dating since 2002 in order to clarify the stratigraphy of the volcano. Appropriate sites were selected based on the age interval of interest (~30 - 150 ka), although some sites could be comprised when the error margin of the age was taken into account. We were limited in the sites that could be chosen for sampling because snow was still present at elevated areas at the time of the year during which the fieldwork was done (April) and because specific sampling sites were located at now inaccessible and/or private areas.

As a result 15 sites were sampled from the lower flanks of the volcano (figure 2.1, table 2.1), of which 12 can be directly found in De Beni et al. (2011) according to the abbreviations therein. For sites DM and IN a second site (the suffix 2 is used, whereas the suffix 1 stands for the original site) was sampled from a lava flow close to the original one. These sites will in the future be subjected to $^{40}Ar/^{39}Ar$ isotopic dating. One other site (OI) was chosen from Del Carlo et al. (2012) and was also subjected to $^{40}Ar/^{39}Ar$ isotopic dating.

In order to find the right sampling sites that were also used for dating, GPS coordinates (UTM-

Site	Age (ka)	2σ (ka)	UTM (m)		Elevation (m a.s.l.)	Reference
AG	154.9	17.0	515373	4160680	5	De Beni et al. 2011
BT	40.9	14.4	482401	4179964	459	De Beni et al. 2011
CS	41.3	6.2	506283	4173509	1361	De Beni et al. 2011
DM1	32.9	10.6	515260	4160697	79	De Beni et al. 2011
DM2	-	-	515287	4160636	77	-
IN1	132.6	4.8	515180	4161960	50	De Beni et al. 2011
IN2	-	-	515256	4161940	9	-
LN	42.1	10.4	492472	4186454	1146	De Beni et al. 2011
MC	28.7	12.6	433749	4180461	599	De Beni et al. 2011
MT	126.4	4.8	511729	4176486	507	De Beni et al. 2011
NA	111.9	9.2	511899	4161715	231	De Beni et al. 2011
OI	28.6	9.4	505054	4195558	557	Del Carlo et al. 2012
RZ	30.8	21.2	497547	4193672	668	De Beni et al. 2011
TC	145.8	14.0	513378	4158379	195	De Beni et al. 2011
VS	121.2	15.0	510912	4158081	366	De Beni et al. 2011

Table 2.1. Overview of the sampled sites. The age including 2σ (if applicable) is determined by the reference that is mentioned in the last column. Universal Transverse Mercator - World Geodetic System 1984 (UTM-WGS84) coordinates (zone 33S) and elevation are measured ourselves but are in good agreement with the corresponding reference.

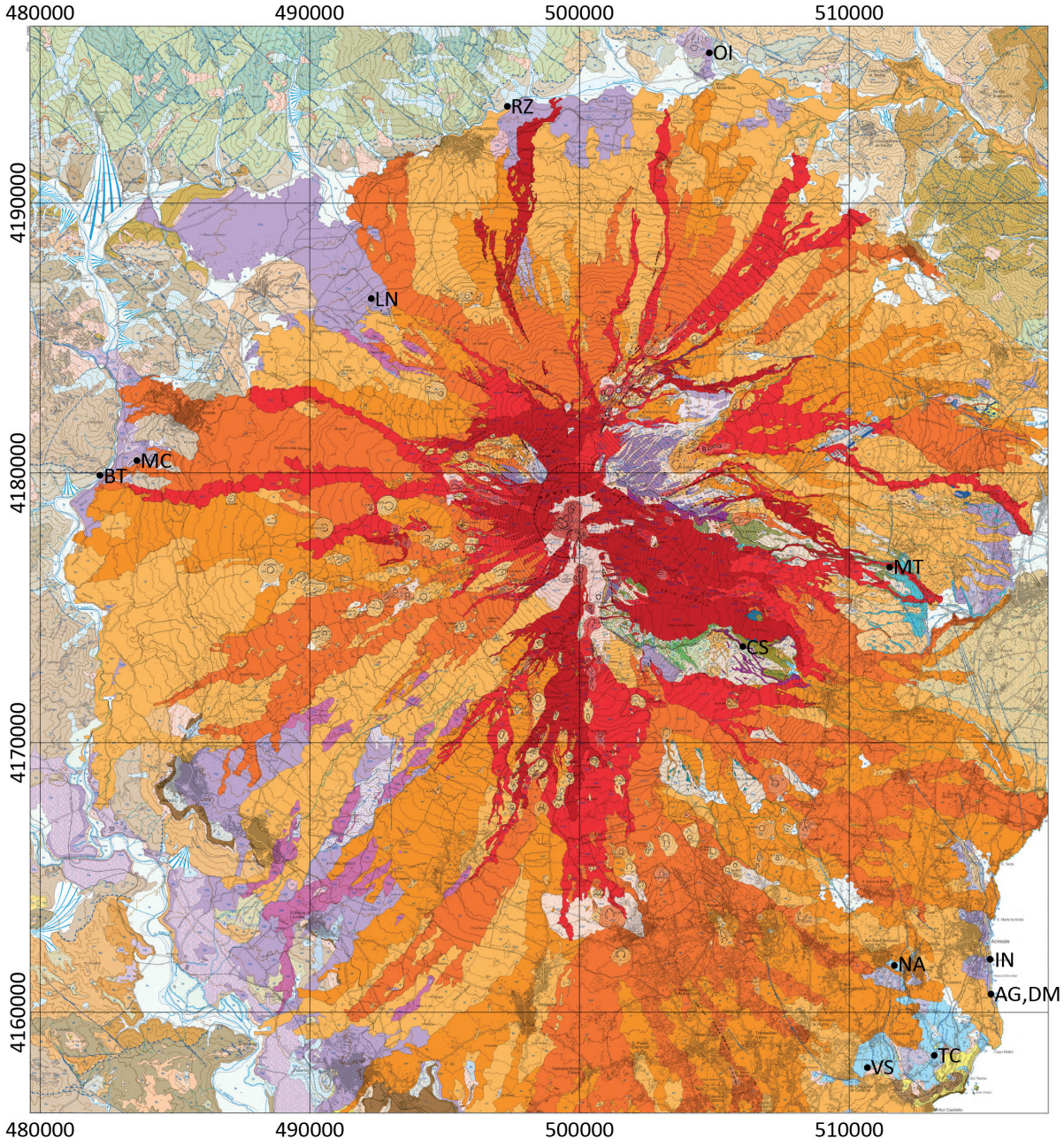

Fig. 2.1. Geological map of Mount Etna, adapted from Branca et al. (2011). Sampling sites are indicated by black dots and the corresponding abbreviation. Coordinates are UTM-WGS84 zone 33S.

WGS84) from De Beni et al. (2011) and Del Carlo et al. (2012) were used. In addition we got help in the field from Stefano Branca, volcanologist from the (Italian) National Institute of Geophysics and Volcanology (INGV), section Catania. He has been involved in all the above mentioned publications on Mount Etna and in particular to the underlying fieldwork.

At each site typically 12 - 15 cores of 5 - 12 cm length and 2.5 cm diameter were drilled, using a water-cooled petrol-powered drill. As much as possible, but at least 8 sample cores were oriented with a magnetic compass. Unfortunately, the weather and other circumstances at the sampling sites did not allow any measurements with a sun compass. Samples were taken from solid parts of the lava flows, generally not too close (> 50 cm) to the top and bottom of the flow. Samples were drilled close to each other to obtain as homogeneous sampling as possible.

3. Methods

3.1. Rock-magnetic analyses

In order to determine the suitability for paleointensity experiments, specimens of all sites were subjected to a series of tests in which some rock-magnetic properties are measured. Information about the thermal susceptibility behavior and the magnetic grain size allow a categorization of the sample sites that is useful in further paleointensity experiments.

3.1.1. Magnetic susceptibility

The magnetic susceptibility χ is the proportionality factor between the magnetization M and the applied magnetic field H (Griffiths, 1999; Tauxe, 2010), giving a measure of the magnetic response to the applied field. In this case it is normalized to the mass of the specimen (~250 - 550 mg of grinded specimen) and therefore it has units of kg^{-1}. The magnetic susceptibility was measured as a function of temperature on an AGICO KLY-3S susceptometer with a CS-3 temperature control unit, also called a Kappabridge. It consists of two coils in one of which a small field is induced by an applied current. Then it measures the offset in the current between measurements with and without the specimen in the other coil; this offset is proportional to the magnetic susceptibility. The specimens are heated during six temperature cycles to progressively higher temperatures up to 600 °C at heating and cooling rates of ~10 °C/min to determine the thermal behavior of the susceptibility.

The alteration temperature can be deduced by looking to the highest temperature that is reached in the last thermal cycle that shows reversible behavior (figure 3.1). The alteration can therefore only be determined with an accuracy of 50 - 100 °C, where we have restricted the maximum alteration to 5%. This is generally the highest temperature that can be used in paleointensity experiments (De Groot, Dekkers, et al., 2012), but other properties have to be looked at as well. When the Curie temperature is reached, the susceptibility drops and the specimen will only exhibit paramagnetic susceptibility. The Curie temperature is determined with the intersecting tangent method (figure 3.1). A specimen can have more than one Curie temperature, at which particular magnetic crystals lose their ferromagnetic behavior (Dunlop and Özdemir, 1997).

Based on the number of Curie temperatures and their magnitude, a categorization into three groups of sites is made. The first category (L) consists of samples with low susceptibility at higher temperatures, i.e. < 20% of maximum susceptibility is left at 200 °C. The second category (H) consists of samples with high susceptibility at higher temperatures, i.e. > 80% of maximum susceptibility is left at 400 °C. Finally, there is a third category (M) with intermediate samples and samples that have a mixed composition and therefore show multiple Curie temperatures.

3.1.2. High-field rock-magnetic properties

In order to determine the high-field rock-magnetic properties, 5 - 6 small specimens (~2 - 10 mg) from each site were measured on a MicroMag, an alternating gradient force magnetometer (PMC Model 2900). It is used to measure both hysteresis loops and back-field remanence curves. From these curves, the necessary parameters for a Day plot can be obtained (Day et al., 1977).

The saturation magnetization M_s, the remanent saturation magnetization M_{rs}, and the coercive force H_c can be deduced from the hysteresis loop. A large external field of maximal 1 T is applied to the

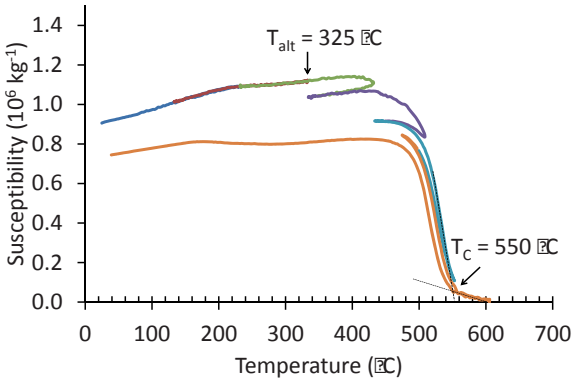

Fig. 3.1. Example of a magnetic susceptibility versus temperature curve. Different colors represent consecutive thermal cycles. The alteration temperature is defined as the highest temperature that is reached in the last thermal cycle which shows maximally 5% alteration. The Curie temperature is determined with the intersecting tangent method.

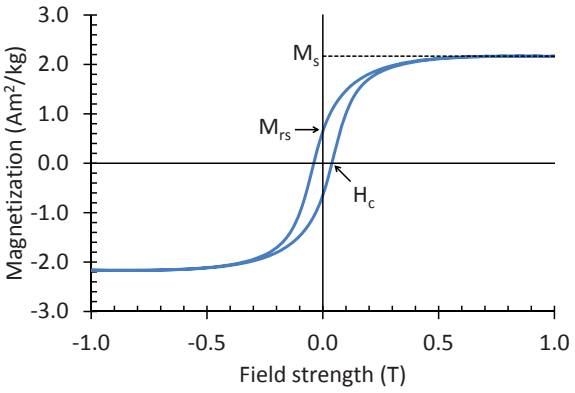

Fig. 3.2. Example of a hysteresis loop, which has been corrected for paramagnetic and/or diamagnetic minerals. The parameters M_s, M_{rs}, and H_c are indicated.

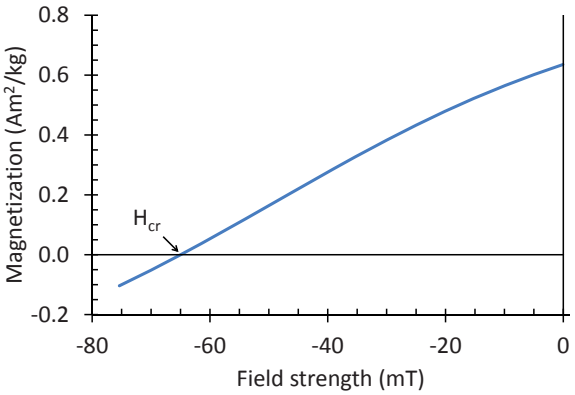

Fig. 3.3. Example of a back-field curve. The parameter H_{cr} is indicated.

specimen to align all magnetic moments in the direction of the applied field and measure M_s. Subsequently, the applied field is decreased stepwise until there is no external field left, at which moment M_{rs} is recorded. A stepwise increase of the external field in the other (negative) direction allows the measurement of H_c, the external field that is needed for zero-magnetization in the specimen. This is repeated in the positive direction, leading to a hysteresis loop (figure 3.2). In the figure, the loop already has been corrected for the presence of paramagnetic and/or diamagnetic minerals that cause the specimen not to saturate (Tauxe, 2010).

The remanent coercive force H_{cr} can be deduced from the back-field curve (figure 3.3). After applying and removing a large external magnetic field that saturates the specimen to M_{rs}, a stepwise increasing magnetic (back-)field is quickly applied and removed in the opposite direction. The back-field for which the net remanence of the specimen is zero, is H_{cr}.

The ratios of M_{rs}/M_s versus H_{cr}/H_c are plotted in a Day plot (Day et al., 1977), giving information about the magnetic grain size distribution. The plot is divided into regions, discriminating between magnetic domain states: single-domain or SD, pseudo-single-domain or PSD, and multi-domain or MD. The magnetic behavior of SD grains is more easy to model and more suitable for paleointensity experiments than PSD and MD grains, where magnetic grains are subdivided into multiple parts by domain walls and exhibit respectively only little or no SD behavior (Dunlop and Özdemir, 1997).

3.2. NRM demagnetization

Specimens of all sample sites were demagnetized to assess their suitability for paleointensity experiments, both thermally and with alternating field (AF) demagnetization. With this demagnetization, possible (viscous) overprints can be detected that might erroneously influence the paleointensity determination. Furthermore, the thermal behavior helps to make a decision if and at which temperature (steps) samples of a particular site should be tested with the different paleointensity methods. AF demagnetization is also used to assess the range of field strengths that is suitable in further experiments.

3.2.1. Thermal demagnetization

Thermal demagnetization was done on three oriented specimens (~2.5 cm diameter, 1 - 1.5 cm length) per site. Sample cores were cut into relatively thin slices in order to stay within the dynamic range of the measurement equipment. Specimens were heated in a magnetically shielded oven (ASC TD-48 SC thermal specimen demagnetizer, residual field in the order of nT) to increasingly higher temperatures. Specimens should be heated at the desired temperature for at least 10 min, depending on the temperature they were heated for 40 - 60 min. After measuring the NRM, temperatures were increased from 100 °C up to 500 °C with 50 °C intervals and from there onward to 600 °C with 25 °C intervals, making a total of 14 temperature steps for each specimen. After heating, specimens were cooled in the oven with a fan back to 30 °C before measuring.

The magnetization was measured in three directions in a 2G DC-SQUID (superconducting quantum interference device) magnetometer. When a specimen is introduced in the system, currents are generated in three sets of superconducting coils that allow for a very accurate full vector measurement. The coils and sensors are protected for other magnetic signals by a superconducting shield, leading to a low noise level. The measured magnetization was corrected for the original orientation of the specimen. Thereafter the declination and inclination were determined and the vector magnetization was plotted in Zijderveld diagrams using the program *Paldir* (figure 3.4). The resulting scalar magnetization was also plotted against temperature to obtain NRM decay curves (figure 3.5).

3.2.2. Alternating field demagnetization

For the alternating field (AF) demagnetization 3 - 6 oriented specimens (again ~2.5 cm diameter, 1 - 1.5 cm length) per site were used, depending on the available material. They were demagnetized in three orthogonal directions by an oscillating field, in 16 increasing steps up to 150 mT. The demagnetization was done in a magnetically shielded environment by AF coils that were in line with the robotized 2G DC-SQUID magnetometer, where the magnetization was measured in three directions after every field step. The resulting magnetization was processed to Zijderveld diagrams (figure 3.4) and NRM decay curves (figure 3.5) as with the thermal demagnetization.

3.2.3. Directions

The obtained directions of both the thermal and AF Zijderveld diagrams are combined to find the mean direction. Depending on the site, 6 - 9 directions were obtained. The mean declination, mean inclination and $\alpha 95$ of these distributions are calculated and the distribution is potentially cut through the Vandamme cut-off in order to remove results that are too far from the mean (Vandamme, 1994). These results are processed to virtual geomagnetic poles (VGPs) and compared with the present day

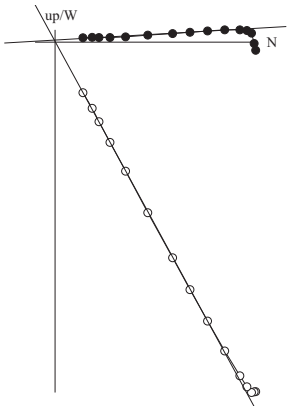

Fig. 3.4. Example of an (AF) Zijderveld diagram. It shows a small overprint that is removed at low AF strengths and decays nicely through the origin.

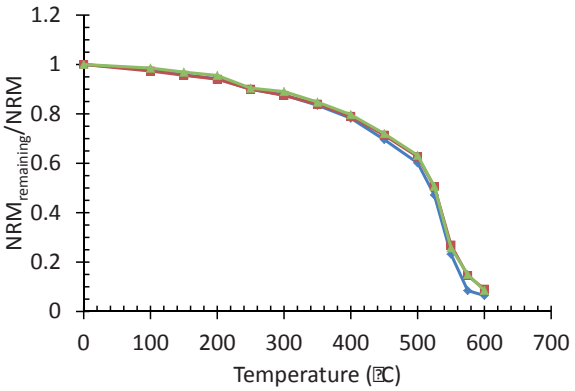

Fig. 3.5. Example of a (thermal) NRM decay curve. The three specimens keep their magnetization up to high temperatures and show mutually similar behavior.

orientation of the Earth's magnetic field.

3.3. Anhysteretic remanent magnetization (ARM) test

De Groot et al. (2012) stated that the domain state corrected multispecimen protocol (*3.4.2 – Multispecimen (MSP) method*) for paleointensity determination could yield varyingly good results when compared with the known natural field (IGRF), implying that the rock-magnetic analyses as described above are not capable of detecting all possible alteration in the examined specimens. Therefore, ARM acquisition curves were obtained to anticipate incipient alteration.

Here we chose to use the 'single core ARM acquisition' as described by de Groot et al. (2012), because long enough drilling cores were available for all sites, the method is far less laborious than the 'aligned ARM acquisition', and the scatter is smaller because of the larger specimen size. Specimens are not first demagnetized by either thermal or AF demagnetization because these processes could both alter the magnetic state of the specimens, although demagnetizing the NRM and acquiring an ARM might not be independent processes when done at the same time.

For each site, 2 - 3 drill cores are marked with a fiducial line before the core is cut into 4 - 8 specimens (again ~2.5 cm diameter, ~1 - 1.5 cm length, 8 - 22 g mass). All specimens are then subjected to an ARM acquisition with respect to the fiducial line. In total 18 increasing steps up to 150 mT were used. One core is not heated, whereas the other core(s) is/are heated to a possible set temperature for the MSP protocol. As long as there is enough material available, two temperatures are tested to find the best set temperature in the MSP experiments. ARM acquisition and magnetization measurements are done in the same setup with a robotized SQUID magnetometer as described for the AF demagnetization.

For half of the specimens (rounded up in case of an uneven number of specimens) no DC bias field was applied, so in fact a single axis AF demagnetization along the direction of the ARM is done. The resulting signal is normalized to the mass of each specimen and averaged per AF level to obtain the specific single axis AF demagnetization (the '0-μT-series'). The other half of the specimens are subjected to a real ARM acquisition with a DC bias field of 35 μT. Again, results are normalized to mass and averaged per AF level to obtain the combined single axis AF demagnetization and ARM acquisition (the '35-μT-series'). The acquired ARM can be calculated by subtracting the 0-μT-series from the 35-μT-series, but has to be corrected for the scatter in the specific NRM (De Groot, Dekkers, et al., 2012).

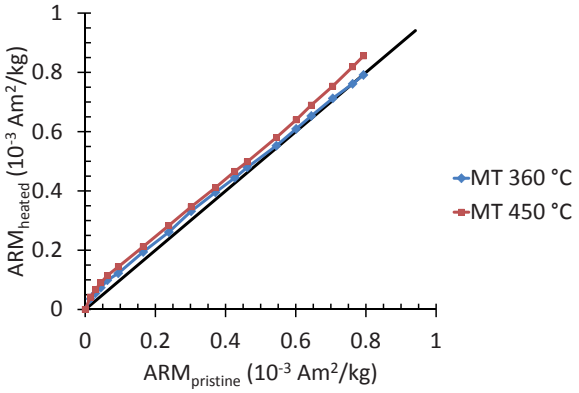

Fig. 3.6. Example of an ARM-test diagram at a bias field of 35 µT. The heated specimens show similar behavior as the pristine specimens. For 360 °C specimens only acquire slightly more ARM at low AF strengths, for 450 °C over the whole range of AF strengths (maximally 150 mT).

The ARM acquisition behavior of the heated specimens is compared with the behavior of the pristine core. When they are plotted against each other, ideally they would end up at the diagonal y = x (figure 3.6). However, when more ARM is acquired after heating, the data will be plotted above the ideal line. In this case more pTRM is expected to be acquired during paleointensity experiments, resulting in an underestimate for the intensity of the field. On the other hand, when less ARM is acquired after heating, the data will be plotted below the ideal line and paleointensity experiments are expected to yield overestimates. The amount of deviation from the ideal behavior led to the choice for one of the used set temperatures or even rejection of the sample site for the MSP experiments.

3.4. Paleointensity determination

After the demagnetization behavior and rock-magnetic properties were obtained, suitable specimens were subjected to several paleointensity methods. In principle, all methods are based on the idea that the ratio between the original NRM and the thermally imparted laboratory TRM should be the same as the fields H_{anc} and H_{lab} that created them (Tauxe, 2010; Dunlop, 2011):

$$H_{anc} / H_{lab} = NRM / TRM \tag{3.1}$$

For this relation to be true, some conditions must be satisfied: NRM and TRM should be (equally) proportional to the magnetic field, TRM should fully replace the corresponding NRM, and the (minerals carrying the) NRM should be magnetically and chemically unaltered since it was created and during all subsequent operations it undergoes. Particularly the alteration during the heating of the specimens forms a major obstacle in determining the paleointensity. New methods have been designed and several adjustments have been made in the classical methods in recent years to avoid this alteration as much as possible (Dunlop, 2011; de Groot, Dekkers, et al., 2012).

In most paleointensity methods the NRM is gradually removed and replaced by a laboratory partial thermoremanent magnetization (pTRM). These pTRMs are artificial as it can only be produced in the laboratory; the Earth's magnetic field cannot be switched on and off during the cooling of a lava flow. However, they are essential in the paleointensity determination and the use of pTRMs relies on some assumptions. Firstly, it is assumed that the blocking temperature T_B at which the pTRM is blocked during cooling, is the same as the unblocking temperature T_{UB} at which the same pTRM is unblocked

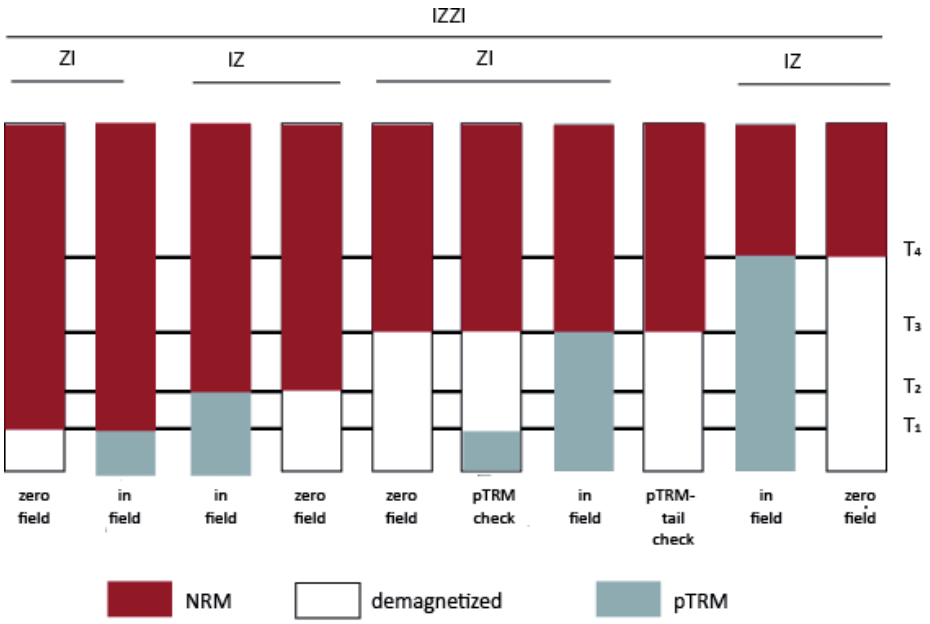

Fig. 3.7. Schematic illustration of the IZZI protocol. The first four temperature steps including the pTRM(-tail) checks of the first full IZZI step are displayed. In this study, the first ZI step is followed by 5 IZZI steps, resulting in eleven temperature steps. The in-field steps were carried out at a field strength of 40 µT. The figure is adapted from Tauxe (2010).

during heating (reciprocity). Then, pTRMs that are created in mutually exclusive temperature ranges should be independent of each other (independence). Finally, these independent pTRMs sum up to the total TRM for the same temperature range (additivity).

3.4.1. Thellier-Thellier method

The classical Thellier-Thellier method (Thellier and Thellier, 1959; from now on simply called Thellier method) was the first extensive method to recover ancient intensities of the Earth's magnetic field (Dunlop, 2011). In this method, the NRM is gradually thermally removed and replaced by a pTRM. The NRM in a specimen can be replaced by a pTRM in several ways. In the original method of Thellier and Thellier (1959) double-heating steps are used, in which the specimen is heated twice to the same temperature. The first time, the specimen is heated and cooled in the laboratory field H_{lab}, whereas it is heated and cooled in the opposite field $-H_{lab}$ the second time. By summation and subtraction of the resulting magnetizations both the NRM remaining and the pTRM gained for each temperature step can be calculated. The method assumes reciprocity, as the magnetization acquired in the first step should be fully removed in the second step and replaced by an opposite magnetization.

In later years, variations of the original protocol were designed. Coe (1967) also used double-heating steps, but introduced the zero-field/in-field method (ZI). A zero-field is used in the first step to directly obtain the remaining NRM and the second (in-field) step allows to calculate the pTRM gained. The contrary is the in-field/zero-field method (IZ), where the first heating and cooling is done in-field, followed by a zero-field step to obtain the NRM remaining and calculate the pTRM gained (Aitken et al., 1988). In all these methods repeated lower temperature steps of in-field heating and cooling (pTRM checks) can be used to assess the remanence carrying capacity of the specimen and prevent the use of any data that is affected by alteration.

These ZI and IZ steps can also be combined to the IZZI method (Tauxe and Staudigel, 2004; Yu et al., 2004). Together with pTRM-tail checks (Riisager and Riisager, 2001), where a zero-field step is inserted

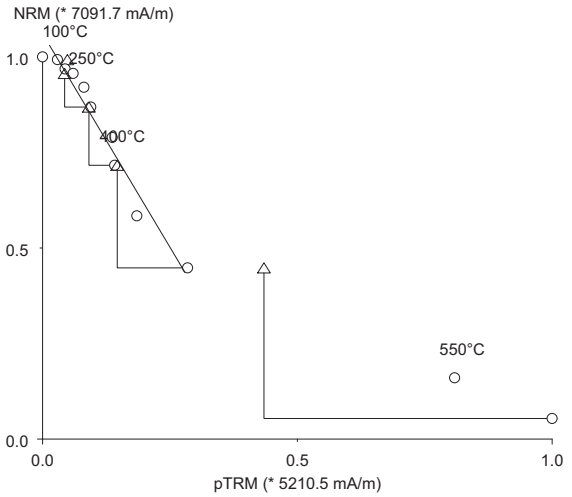

Fig. 3.8. Example of an Arai diagram. The NRM remaining is plotted against the pTRM gained for every temperature step (circles), for some of which the temperature is given. The pTRM checks are plotted against the NRM that it is supposed to check (triangles); the line connects the check to the last regular temperature step that is measured before the check. The pTRM check after 500 °C is the last good check, so the higher temperature points are discarded for the linear fit. The paleointensity can be calculated by multiplying the slope of the linear fit with the applied field.

between the ZI an IZ steps, this method is highly sensitive to the presence of pTRM tails. These pTRM tails are created if a pTRM is not fully removed when heating again to the same temperature in a zero-field environment.

In this study the IZZI protocol is used as it is the most complete method to detect any alteration (Yu et al., 2004). After measuring the NRM, a first ZI step is followed by five consecutive IZZI steps including pTRM(-tail) checks (figure 3.7). Based on both the demagnetization and rock-magnetic properties, a subdivision in two groups with different temperature steps was made; a group with temperature intervals of 40 °C (80 - 480 °C) and a higher temperature group with intervals of 50 °C (100 - 600 °C). For each site 4 - 5 specimens were used, dependent on the available material. As with demagnetization, the specimens were heated in a magnetically shielded oven. In this oven it was also possible to apply a magnetic field of 40 µT parallel to the axial direction of the oven for the in-field steps. The magnetization of the specimens was then measured in three directions in the SQUID magnetometer.

The obtained data is then plotted in a so-called Arai diagram, where the NRM remaining is plotted against the pTRM gained (figure 3.8). The paleointensity then is determined by calculating the slope of the linear fit through the data points and multiplying its absolute value with the magnitude of H_{lab}. When this is equal to the ancient field H_{anc}, the slope of the linear plot should be -1 (equation 3.1).

The pTRM(-tail) checks are also plotted in the Arai diagram (Leonhardt et al., 2004; Tauxe, 2010). The pTRM gained for the pTRM check is plotted against the earlier measured NRM that it is supposed to check. When the specimen has not been subject to alteration, the measured pTRM should be the same as for the original measurement. However, when alteration has taken place, the pTRM check is shifted to the left or right with respect to the original measurement.

The pTRM-tail checks are generally plotted along the x-axis as the magnitude of the difference between the check and the original zero-field step against the pTRM gained that is measured at the same temperature (Tauxe, 2010). When this yields a negative value, it is the result of a low-temperature tail, which corresponds to a portion of the pTRM lost by heating to temperatures below the blocking temperature. On the other hand, a pTRM could persist to temperatures higher than the blocking tem-

	N	β	f	q	α (°)	MAD (°)	DRAT (%)
SELCRIT-1	≥ 4	≤ 0.1	≥ 0.15	≥ 1	≤ 15	≤ 15	≤ 10
PICRIT-03	≥ 4	≤ 0.1	≥ 0.35	≥ 0.2	≤ 15	≤ 15	≤ 7

Table 3.1. Selection criteria (mentioned in the text) that were used in the Thellier experiments. SELCRIT-1 criteria come from Selkin and Tauxe (2000), PICRIT-03 criteria come from Kissel and Laj (2004).

perature. This gives rise to a high-temperature tail, which can be seen as pTRM-tail checks above the x-axis. This is particularly the case for non-SD grains, and is also displayed as sagging of the data points below the ideal linear line.

These Arai diagrams are plotted with the program ThellierTool (Leonhardt et al., 2004). This program allows the use of full vector analysis for all experiments, including the checks that are mentioned above. It also calculates a wide range of parameters that can be used to further analyze the results of the Thellier experiments (Coe et al., 1978; Selkin and Tauxe, 2000; Leonhardt et al., 2004). These include the number of data points N, the standard deviation divided by the slope of the linear fit β, the fraction of NRM f, the quality factor q, the angular difference between anchored and not-anchored solution α, the maximum angular deviation MAD, and the deviation of the pTRM check from its corresponding pTRM normalized to the length of the segment DRAT.

Based on the aforementioned parameters, Biggin et al. (2007) proposed some sets of selection criteria to strip out the most inaccurate paleointensity determinations: SELCRIT-1 (Selkin and Tauxe, 2000) and PICRIT-03 (Kissel and Laj, 2004). PICRIT-03 is generally stricter than SELCRIT-1, especially for the fraction of NRM and the maximum angular deviation, but somewhat less strict in the quality factor (table 3.1). However, these sets do not quantify any criteria on the pTRM-tail checks and might therefore not detect sagging, caused by MD behavior. Therefore, the tail parameter normalized to the NRM δt* (Leonhardt et al., 2004) is checked separately. The threshold they use for class B (δt* < 5) is used as a directive for both sets of selection criteria here.

3.4.2. Multispecimen method

Although pTRM(-tail) checks are introduced in the different Thellier protocols, it is still prone to the risk of alteration, especially by the large number of heating steps that are involved. One of the methods to avoid this large number of heating steps is the multispecimen protocol (MSP), which is based on the linearity of the gained pTRM with the applied field (Dekkers and Böhnel, 2006; Fabian and Leonhardt, 2010). In this method multiple specimens are subjected to the same measurements and a reduced number of heating steps. Instead of heating a single specimen to increasingly higher temperature steps, several groups of multiple specimens are heated to different field strengths at the same temperature.

In the original MSP-DB (Dekkers and Böhnel, 2006), sister specimens are heated to the same temperature (the set temperature) only once. Several specimens are during the heating subjected to different laboratory fields that are applied parallel to the NRM of the specimens. Based on the symmetry relation of Biggin and Poidras (2006) the laboratory field for which the sum of the remaining NRM and gained pTRM is equal to the original NRM, is considered to be equal to the ancient field (figure 3.9). In order to determine this field, the ratio of the pTRM to the NRM, Q_{DB} = (pTRM - NRM) / NRM, is plotted against the applied field and a linear fit is made through the data points (figure 3.10). The field strength at which the linear fit intersects the x-axis is the estimated paleofield and the confidence interval is gi-

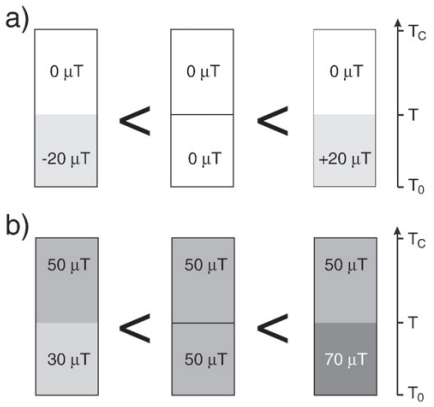

Fig. 3.9. The principle of the MSP method. In a) the trivial inequality can be seen between heating a non-magnetized specimen from room temperature T_0 to temperature $T < T_C$ in a negative field, a zero-field, and a positive field. Assuming the symmetry relation of Biggin and Poidras (2006), shifting this situation by 50 µT leads to b). The laboratory field for which the magnetization remains equal after heating, is assumed to be the paleofield. Figure from Fabian and Leonhardt (2010).

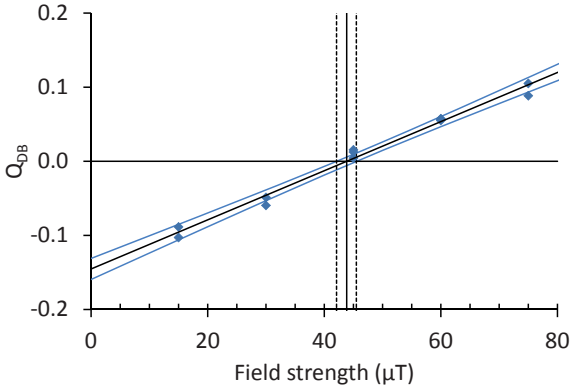

Fig. 3.10. Example of a MSP(-DB) plot. The ratio Q_{DB} is measured for two to three specimens (blue diamonds) per field strength. The intersection of the linear fit through the data points (black line) with the x-axis determines the paleointensity. The confidence interval is determined by the intersection of the uncertainty envelope (blue lines) with the x-axis.

ven by the intersection of the uncertainty envelope with the x-axis. A relatively steep intersection with a small error envelope is desirable for a good estimate (De Groot, Dekkers, et al., 2012). Therefore, a set temperature should be chosen at which a sufficient amount of the NRM is removed but also in this method the temperature should not be too close to the alteration or Curie temperature to avoid any alteration effects.

The advantages of the MSP-DB protocol should be that magnetic history and alteration effects are eliminated by a single heating at relatively low temperature, that specimens with MD grains could equally be used in the experiments, and that the protocol is far less laborious than the Thellier protocols (Dekkers and Böhnel, 2006). However, Fabian and Leonhardt (2010) doubted the statement of magnetic domain state independence. They proposed an extended protocol that should make it possible to check for potential domain-state and tail effects: the MSP-DSC (domain state corrected) protocol.

This protocol includes three further heating steps to correct for these effects and find the domain state corrected ratio Q_{DSC} (figure 3.11). After the first heating step from the MSP-DB protocol with the applied field parallel to the NRM of the specimen, a second step is introduced at the same temperature but with the field antiparallel to the specimen. This is done to determine a slope correction. The third step is a zero-field heating to detect possible domain state effects, whereas the fourth step is the same as step 1 to check for any alteration with the relative alteration error $\varepsilon_{alt} = |(m_1 - m_4) / m_1|$. Although these extra steps imply an extra possibility for alteration and magnetic treatment history, the corrections of this protocol show promising results.

Based on the results of the ARM acquisition and the other tests to check for the suitability of the sample sites, specimens were subdivided into two groups with different set temperatures. For each examined site 2 - 3 specimens were used per field step and 4 - 5 field steps were used per site. After measuring the NRM of the specimens, declination and inclination were calculated in order to align the specimens during heating. Heating was again done in a magnetically shielded oven, but the magnetization of the specimens was measured by an AGICO JR-6 dual speed spinner magnetometer. In this magnetometer the specimen is rotated at a constant angular speed inside a pair of coils, in which an

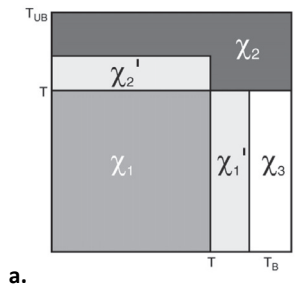

a.

In **a.** a simplified representation to describe the remanent magnetization is shown (Fabian and Leonhardt, 2010). Heating in a zero-field to T unblocks all remanences with $T_{UB} < T$. Subsequent cooling in a field H magnetizes all grains with $T_B < T$. Therefore, the remanent magnetization need not follow the symmetry relation of Biggin and Poidras (2006) in figure 3.7. The region depicted by χ_1 depicts the pTRM gained, whereas χ_2 shows the NRM remaining and χ_3 the part that is not remagnetized after unblocking. The region χ_1' displays the effect of in-field heating (Biggin and Poidras, 2006) and region χ_2' the tail of pTRM.

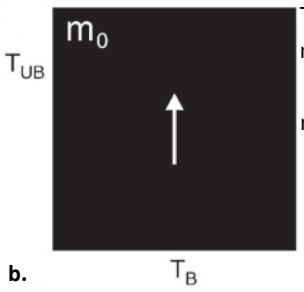

b.

The original NRM is displayed in **b**. Using the representation of **a.** the original magnetization m_0 can be expressed as

$$m_0 = \chi_1 H_{anc} + \chi_2 H_{anc} + \chi_3 H_{anc} + \chi_1' H_{anc} + \chi_2' H_{anc}. \quad (3.2)$$

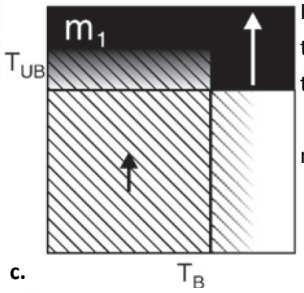

c.

In **c.** the single heating step of the MSP-DB protocol is showed, which is also the first step of the MSP-DSC protocol. After heating and cooling the specimen in a laboratory field H_{lab} parallel to the original NRM the remanent magnetization m_1 is given by

$$m_1 = \chi_1 H_{lab} + \chi_2 H_{anc} + \chi_1' H_{lab} + \chi_2' H_{lab}. \quad (3.3)$$

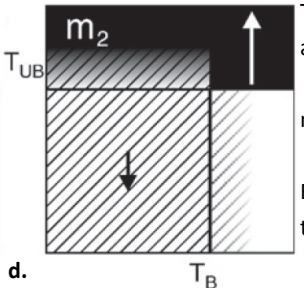

d.

The second step of the MSP-DSC protocol (**d.**) is similar to the first, but with the laboratory field antiparallel to the original NRM. The remanent magnetization m_2 is given by

$$m_2 = \chi_1 H_{lab} - \chi_2 H_{anc} - \chi_1' H_{lab} - \chi_2' H_{lab}. \quad (3.4)$$

By adding m_1 and m_2, a slope correction can be made for the NRM fraction f that is demagnetized.

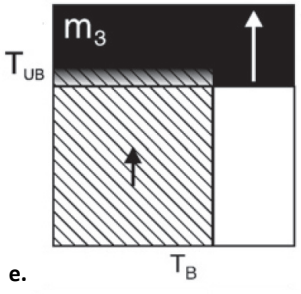

e.

In step three (**e.**) the specimen is heated in zero-field and cooled in the laboratory field parallel to the orginal NRM, in order to detect the effects of the domain state by comparing m_1 to

$$m_3 = \chi_1 H_{lab} + \chi_2 H_{anc} + \tfrac{1}{2}\chi_2' H_{lab}. \quad (3.5)$$

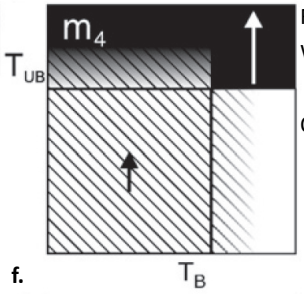

f.

Finally, the first step is repeated (**f.**) to provide relative alteration error $\varepsilon_{alt} = |(m_1 - m_4) / m_1|$. With these magnetizations, the domain state corrected ratio can be calculated:

$$Q_{DSC} = ([1 + \alpha]m_1 - m_0 - \alpha m_3) / (m_0 - \tfrac{1}{2}m_1 - \tfrac{1}{2}m_2) \quad (3.6)$$

Fig. 3.11. Phenomenological visualization and calculations of the MSP-DSC protocol. Figures from Fabian and Leonhardt (2010).

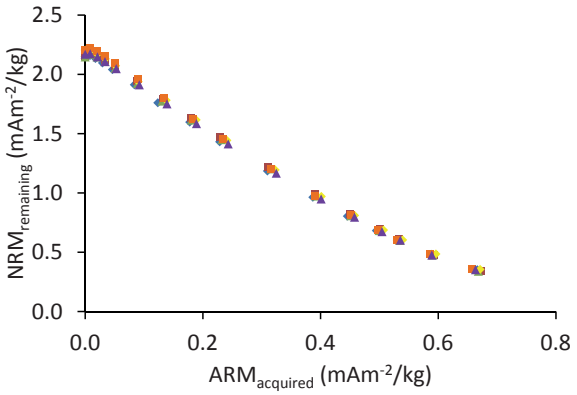

Fig. 3.12. Example of an ARM Arai diagram. Six specimens are subjected to the measurements. A small overprint is removed at low AF strengths and not used for the linear slope that determines the pTh-slope. Furthermore, the AF-ARM versus AF-NRM diagram is evaluated to check whether the same magnetic grains are (de)magnetized (after) during the ARM acquisition.

alternating current is induced. From this current the remanent magnetization in the plane perpendicular to the axis of rotation can be deduced. By using the MSP-DSC protocol, the MSP-DB is followed at the same time as the former protocol is just an extension of the latter. In this way, both protocols can be compared to each other. For all calculations regarding the MSP-DSC protocol the standard value of 0.5 is used for the fraction α (Fabian and Leonhardt, 2010).

3.4.3. Pseudo-Thellier method

The pseudo-Thellier method is not an absolute but a relative paleointensity method. Tauxe et al. (1995) presented a method to normalize sedimentary records for estimating the relative paleointensity of the geomagnetic field. The essence of the method is to compare the demagnetization in a specific coercivity interval directly with the acquisition of an ARM in the same interval. As it relates the relative ability of a specimen to acquire an ARM, it is a relative instead of an absolute method to determine the paleointensity. It has the advantage that specimens are not heated, that it should be possible to remove viscous components from the original magnetization, and that there is a measure of the uncertainty in the individual relative paleointensity determination.

However, the pseudo-Thellier method was never applied to lavas until recently. An unpublished study of De Groot, Biggin, et al. (2012) examined this method on recent lavas from Hawaii. It lead to promising results when values were compared to known IGRF-values of the geomagnetic field. Furthermore, it allows for a distinction between reliable results and possible under- or overestimates of the paleointensity.

The pseudo-Thellier method consists of three steps. The first step is to AF demagnetize the specimens in three orthogonal directions. This is already done for AF demagnetization (*3.2.2. – Alternating field demagnetization*), so the same specimens (3 - 6 specimens per site, ~2.5 cm diameter, 1 - 1.5 cm length) can be used in subsequent steps. Secondly, an ARM acquisition is done comparable to the ARM-test for the MSP method, with the difference that now the specimens are demagnetized beforehand, all specimens are subjected to the bias field, and the bias field is 40 µT. The ARM acquisition data is plotted against the remaining NRM for every of the 16 field steps (figure 3.12) in an Arai diagram. From this plot a linear fit can be made, of which the slope is called the pseudo-Thellier (pTh-)slope. In order to determine this slope, lower steps removing viscous components and higher steps leaving too few NRM might be discarded.

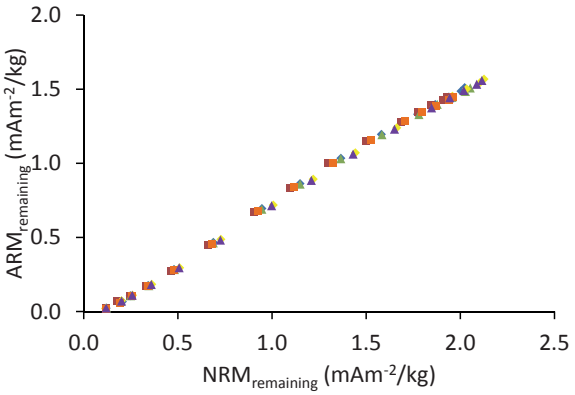

Fig. 3.13. Example of an AF-ARM versus AF-NRM diagram. Six specimens are subjected to the measurements. It shows perfect linear behavior, indicating the magnetization is carried by the same magnetic grains after the ARM acquisition.

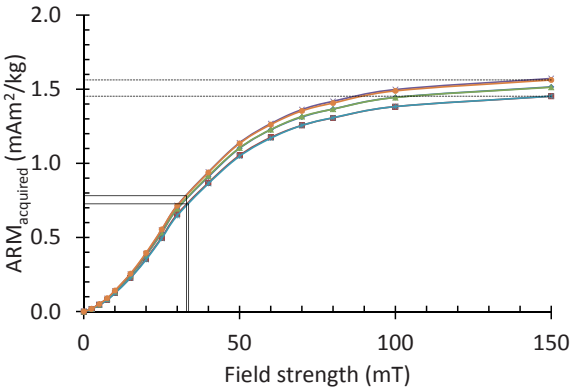

Fig. 3.14. Example of an ARM acquisition curve. Six specimens are subjected to the measurements. Although a small difference occurs in the acquired ARM at 150 mT, the shape of the curves are similar. For both high and low ARM at 150 mT (dotted lines), the parameter $B_{1/2}$ at which half of the ARM is acquired (solid lines) is almost equal.

Two types of tests are done to assure the right pTh-slope is used. Firstly, the specimens are again AF demagnetized (AF-ARM) and the resulting magnetizations are plotted against the original AF demagnetization (AF-NRM) to check whether the same magnetic grains are demagnetized after (and thus also magnetized during) the ARM acquisition (figure 3.13). The Zijderveld diagrams are investigated to prevent overprints from being used. The part of the field that constitutes the linear part in the Arai diagram and is not affected by overprints is accepted to determine the pTh-slope.

Furthermore, pseudo-Thellier results depend on the grain size distribution in the samples (Yu et al., 2003). Therefore, the parameter $B_{1/2}$ (the applied field for which half of the saturated ARM is imparted into a specimen) is determined (figure 3.14). This parameter is a measure of the grain size. According to De Groot, Biggin, et al. (2012) only specimens with 23 mT < $B_{1/2}$ < 63 mT are reliable for paleointensity determination with this method. Generally specimens are saturated at an applied field of 150 mT, but this should be checked as higher fields might be necessary.

The pTh-slope is a relative measure of the paleointensity and should be related to absolute values. Based on the known IGRF-values of the intensity for the historical samples from Hawaii that were investigated by De Groot, Biggin, et al. (2012), the pTh-slopes are calibrated to absolute paleointensities.

4. Results

4.1. Rock-magnetic analyses

4.1.1. Magnetic susceptibility

Measurements of the magnetic susceptibility on the Kappabridge show varied behavior between the different sites when plotted against the temperature (figures A1.1a-15a, table 4.1). Alteration temperatures vary roughly between 225 °C and 425 °C, but it should be noted that this is a lower limit as alteration occurs somewhere during one of the thermal cycles (50 - 100 °C). The alteration temperature is chosen to be the highest temperature of the last cycle where < 5 % change in susceptibility occurs. Curie temperatures also vary widely between 125 °C and 550 °C. Furthermore, some sites clearly show multiple Curie temperatures, representing multiple magnetic components in the sample.

Based on the number of Curie temperatures and their magnitude, a categorization into three groups of sites is made. The first category (L) consists of three samples (BT, DM1, and RZ) with low susceptibility at higher temperatures, i.e. < 20% of maximum susceptibility is left at 200 °C (e.g. figure 4.1a). These sites all show an alteration temperature of 225 °C and Curie temperatures between 125 °C and 200 °C, indicating a more titanium-rich titanomagnetite composition (Dunlop and Özdemir, 1997).

The second category (M) also consists of three samples (IN1, LN, and TC) with intermediate behavior (e.g. figure 4.1b). These samples all show multiple Curie temperatures and therefore a mixed composition of grains with different titanium-iron ratios. Alteration temperatures are not high with values between 225 °C and 325 °C.

The last category (H) consists of samples with high susceptibility at higher temperatures, i.e. > 80% of maximum susceptibility is left at 400 °C (e.g. figure 4.1c). This category is the largest with 9 samples: AG, CS, DM2, IN2, MC, MT, NA, OI, and VS. These sites have the highest dominant Curie temperature (500 °C - 550 °C), slightly below the Curie temperature of pure magnetite. However, some sites show a gradual decay of susceptibility with temperature, indicating a broad spectrum of titanium-iron ratios in the magnetic grains. Sites from this group also generally show higher alteration temperatures between 325 °C and 425 °C and therefore seem most promising for paleointensity experiments.

4.1.2. High-field rock-magnetic properties

When the ratios of M_{rs}/M_s versus H_{cr}/H_c from the hysteresis loops and back-field curves are plotted in a Day plot (figure 4.2), it can be seen that all sites show pseudo-single-domain behavior. Sites from groups L and M tend to be most towards the MD area with $0.07 < M_{rs}/M_s < 0.18$ and $2.4 < H_{cr}/H_c < 3.8$,whereas the sites from group H are plotted in the direction of the SD area with $0.14 < M_{rs}/M_s < 0.33$ and $1.5 < H_{cr}/H_c < 2.5$. Some overlap occurs mainly in the ratio of M_{rs}/M_s as DM1 yields a rather high value of 1.8.

A large variation occurs in the magnitude of the error margins. Sometimes single values even differed more than two standard deviations from the average of 6 samples, so it was decided not to take these results into account. This was the case for sites IN1 and MT. For other sites such as AG, BT, and DM1 large variations occurred as well, but not single values that differed largely from the average. This large variation is reflected in the large error margins and can be a sign of heterogeneity in the samples since only very small samples are used.

Site	T_{alt} (°C)	T_{C1} (°C)	T_{C2} (°C)	T_{C3} (°C)	Category
AG	325	525			H
BT	225	200			L
CS	325	550			H
DM1	225	125			L
DM2	425	550			H
IN1	225	225	400		M
IN2	425	550			H
LN	325	300	500		M
MC	325	500			H
MT	325	550			H
NA	425	550			H
OI	325	550			H
RZ	225	125			L
TC	325	125	400	550	M
VS	325	550			H

Table 4.1. Alteration and Curie temperature(s) from the magnetic susceptibility versus temperature curves and the resulting category. The different categories are mentioned in the text.

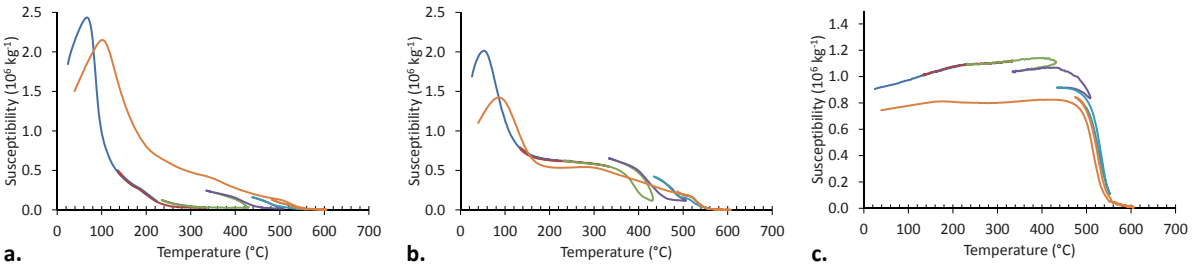

Fig. 4.1. Magnetic susceptiblity curves of three representative sites for groups L (**a.**), M (**b.**), and H (**c.**). Group L (site RZ) loses > 80% of its susceptibility at 200 °C and has a low Curie temperature of 125 °C. Group M (site TC) shows multiple Curie temperatures: 125 °C, 400 °C, and 550 °C. Group H (site MT) has > 80% of its susceptibility left at 400 °C and has a high Curie temperature of 550 °C. Alteration is revealed when a thermal cycle shows non-reversible behavior.

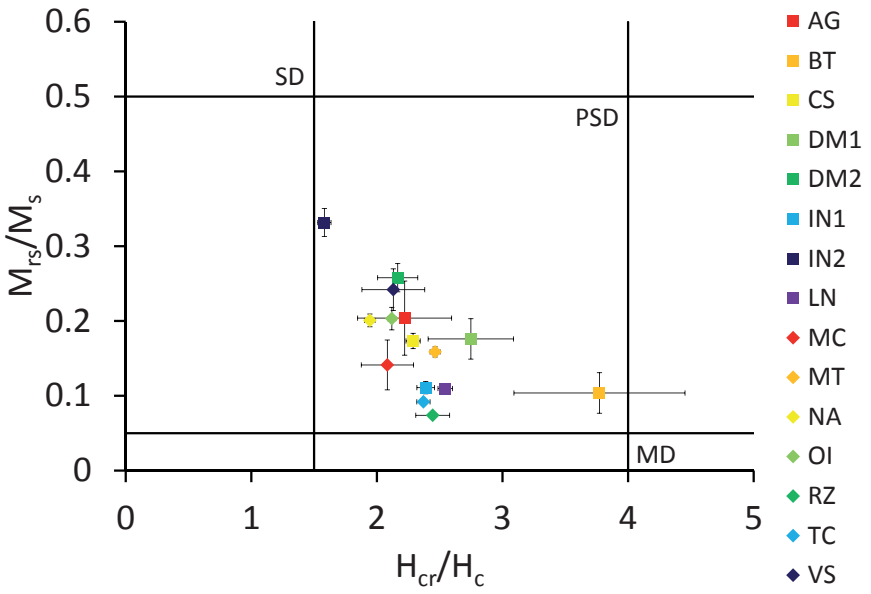

Fig. 4.2. Day plot with all sites. All sites yield PSD behavior, the sites of group H tending to be most towards SD. The error bars depict one standard deviation uncertainty.

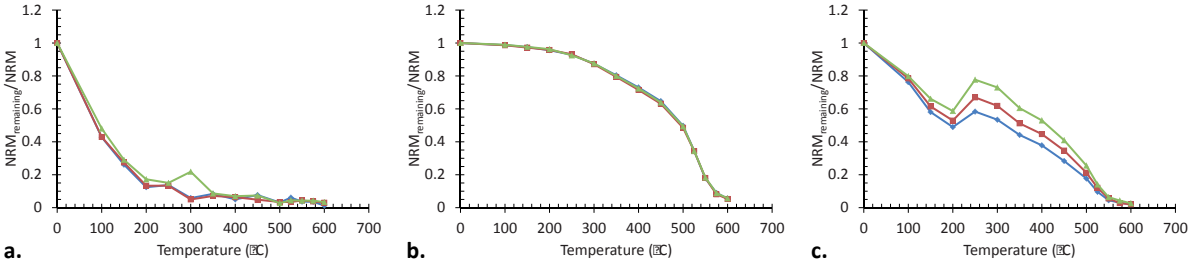

Fig. 4.3. Thermal NRM decay curves of three sites. Site RZ (**a.**) shows a rapid decay, which is common for sites of groups L and M. Site OI (**b.**) keeps a magnetization up to high temperatures and mutually very similar behavior, which is characteristic for a part of group H. Site CS (**c.**) is typical for the other part of group H, which more quickly loses its magnetization. Furthermore, mutual differences exist between the specimens and a remarkable increase in magnetization can be seen at 250 - 300 °C.

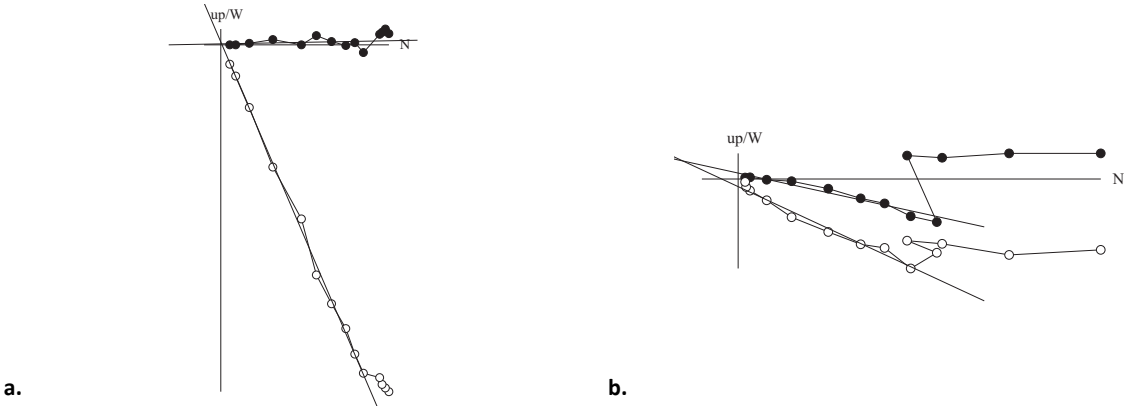

Fig. 4.4. Thermal Zijderveld diagrams of two sites. Site OI (**a.**) shows a small overprint but otherwise good behavior as it decays nicely in a straight line through the origin so the directions can easily be obtained. Site CS (**b.**) shows a large overprint that seems to be removed at 250 - 300 °C. It does not decay nicely through the origin, so directions are more difficult to obtain.

4.2. NRM demagnetization

4.2.1. Thermal demagnetization

From the thermal NRM decay curves (figures A1.1b-15b) we see that the sites also show varied behavior when thermally demagnetized. Generally, sites from groups L and M (e.g. figure 4.3a) lose their magnetization much faster than the sites from group H (e.g. figure 4.3b), although there are some differences within group H. Sites CS, DM2, MC, and VS (e.g. figure 4.3c) from group H lose their magnetization in a similar way as most sites from groups L and M, whereas the other sites from this group (AG, IN2, MT, NA, and OI) keep a magnetization close to the NRM up to higher temperatures. At the maximum temperature of 600 °C, the magnetization is reduced to ≤ 5% of the NRM for all sites.

In about two-third of the sites (BT, IN1, IN2, MT, NA, OI, RZ, TC, and VS), specimens within one site show very similar behavior when normalized to the NRM (e.g. figure 4.3b). For some sites (AG, CS, DM1, DM2, LN, and MC) however, some variation occurs (e.g. figure 4.3c) although the shape of the decay curves are more or less similar. This trend might have been less pronounced when samples would have been normalized to their mass because possible overprints influence the normalization to the NRM. Furthermore, a significant increase in magnetization can be seen in about one-third of the sites at a temperature of 250 - 300 °C (e.g. figure 4.3c). Although the size of the increase differs between sites, the temperature at which it occurs is the same.

Furthermore, results were plotted in Zijderveld diagrams (figures A2.1a-15a), from which the orientation of the field can be deduced. The scatter in these diagrams is quite large as the samples are

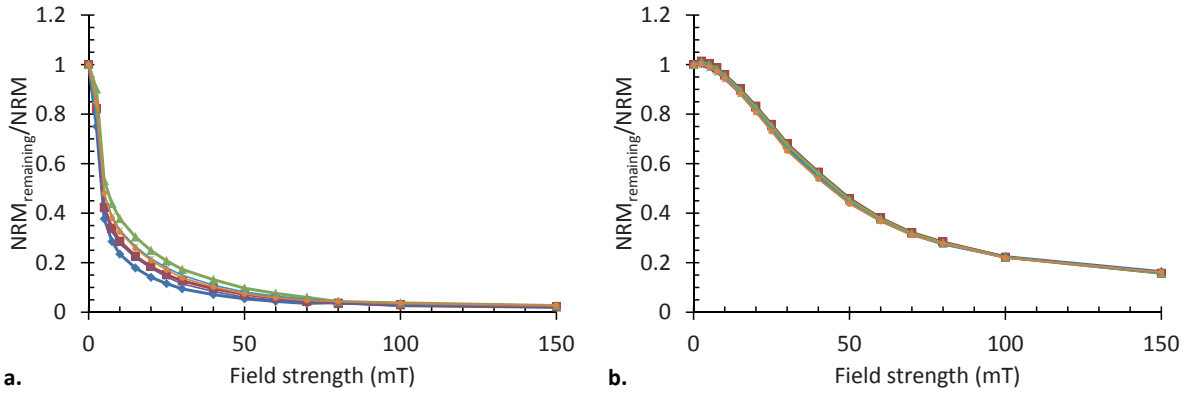

Fig. 4.5. AF NRM decay curves of two sites. Site CS (**a.**) quickly loses its magnetization, which is characteristic for sites that also thermally get quickly demagnetized. Site OI (**b.**) stays magnetized up to higher field strengths and has even ≥ 15% left at 150 mT. This behavior is generally seen for sites that keep a high magnetization up to high temperatures.

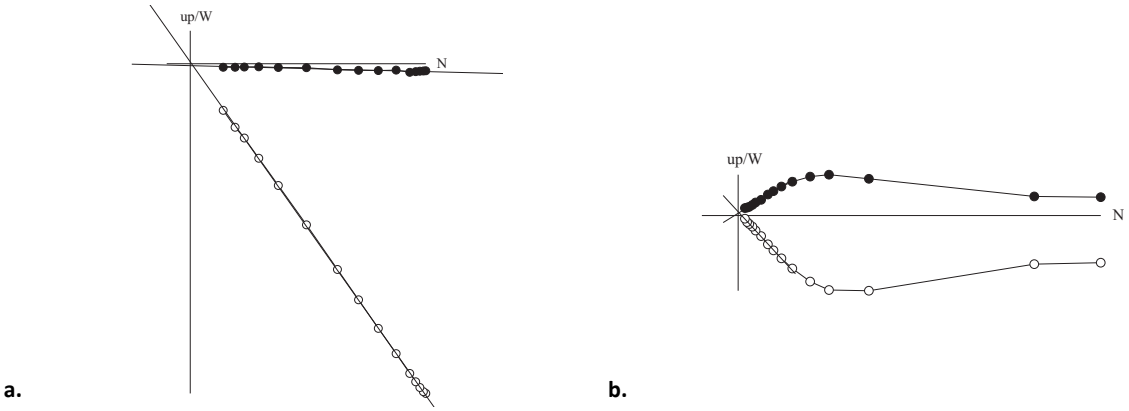

Fig. 4.6. AF Zijderveld diagrams of two sites. Site IN2 (**a.**) shows almost perfect behavior and decays straight through the origin. Site CS (**b.**) shows again a large overprint that seems to be removed at 15 mT.

measured manually in contrast to the robotized measurements for AF demagnetization. For about two-third of the samples directions could be reasonably determined from the Zijderveld diagrams (e.g. figure 4.4a). For the other part (CS, DM1, DM2, RZ, TC, and VS) it was quite difficult or almost impossible to obtain any direction of the magnetization because of large overprints (e.g. figure 4.4b). The increase in magnetization in the NRM decay curves is also clearly visible as a change in the direction of the magnetization in the Zijderveld diagrams at the same temperature (250 - 300 °C).

4.2.2. Alternating field demagnetization

There is a clear correlation between the NRM decay curves of the thermal demagnetization and of the alternating field demagnetization (figures A1.1c-15c). Sites that are easily thermally demagnetized also quickly lose their magnetization due to AF demagnetization (e.g. figure 4.5a) down to only a few percent. The same sites that keep a high magnetization up to high temperatures (AG, IN2, MT, NA, and OI) also keep a high magnetization up to higher AF strengths (e.g. figure 4.5b). They generally have a higher NRM remaining at 150 mT, up to ≥ 15% for site OI.

In AF demagnetization less within-site variation occurs than in thermal demagnetization. The main exceptions are sites DM2 and VS, although the shape of the decay curves for different specimens are quite similar. This can again be explained by the overprints that affect the normalization to the NRM. No increase of the magnetization is visible in these decay curves except for site VS, where the increase

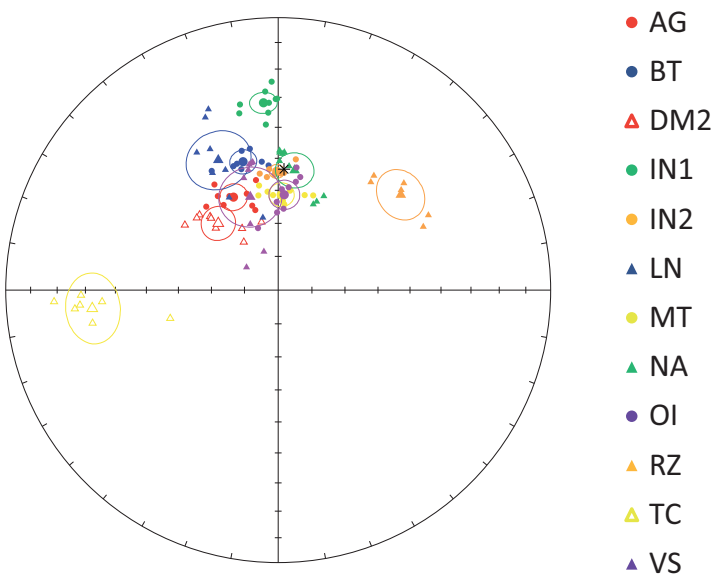

Fig. 4.7. Equal area plot showing declinations and inclinations using both thermal and AF demagnetization. Closed circles indicate sites with $\alpha_{95} < 5°$, whereas (open) triangles indicate sites with $5° < \alpha_{95} < 10°$ (and a negative inclination). Sites with $\alpha_{95} > 10°$ are omitted. Lines represent the corresponding α_{95} and the asterix represents the present day field direction at Mt. Etna.

is visible at a field strength of 10 - 20 mT. This does not seem to be related to the increase in magnetization in the thermal decay curves, as VS was not one of the sites where this phenomenon occurred.

When plotted in Zijderveld diagrams (figures A2.1b-15b), AF demagnetization shows much smoother behavior than thermal demagnetization. This is partly because of the robotized measurements, but also thermal effects such as alteration and remagnetization are omitted. On the other hand, small errors by imperfectly aligned samples are not leveled out by the scatter of manual measurements. For the sites with a reasonable orientation from the thermal Zijderveld diagrams, an orientation can be deduced as well easily from the AF Zijderveld diagrams (e.g. figure 4.6a). For the other sites (e.g. figure 4.6b) a clear change in orientation occurs during the demagnetization, indicating the removal of an overprint.

4.2.3. Directions

In general, directions obtained from thermal and AF demagnetization were consistent (figure 4.7). As discussed before, especially directions from thermal demagnetization were sometimes difficult to obtain. For sites LN, RZ, and TC this lead to devious results, that were cut off by the Vandamme cut-off. For sites CS, DM1, and MC scatter was high in general with no particular outliers; they are omitted because $\alpha_{95} > 10°$. In some cases (sites DM2, IN1, IN2, MT, NA, and VS) the directions obtained by thermal demagnetization differ from those obtained by AF demagnetization. However, a mean could be calculated with $\alpha_{95} < 10°$ and these sites are not necessarily the sites with the highest α_{95}.

Most of the remaining sites have an orientation that is near the present day orientation of the Earth's magnetic field. Site RZ clearly deviates, but it has a positive inclination like the present day field. Sites DM2 and TC have negative inclinations and differ even more from the present day field. Results are processed to VPGs to investigate the effect of these orientations on the virtual pole (figure 4.8). Now we see that most sites have a pole with latitude > 67°, which has been observed in the last centuries. Site RZ has its pole at a latitude of about 44° in present day China, which is an indication for an

Site	Dec (°)	Inc (°)	α_{95} (°)	VGP_{Lat} (°)	VGP_{Long} (°)	n (rejected)
AG	334.1	58.9	4.1	69.7	-60.9	9
BT	344.6	49.6	3.8	75.3	-100.7	8
DM2	317.9	-63.2	5.1	-0.6	-136.3	9
IN1	355.4	31.6	3.6	69.1	-152.4	9
IN2	359.2	54.1	2.2	87.0	-152.3	9
LN	335.2	46.3	9.2	66.9	-93.9	8 (1)
MT	1.9	61.3	3.7	85.1	31.7	9
NA	7.8	53.4	5.5	82.7	132.7	9
OI	3.6	61.3	4.5	84.7	45.4	9
RZ	52.1	42.4	7.3	44.1	106.2	6 (1)
TC	264.3	-32.1	9.3	-14.9	-85.5	7 (2)
VS	343.2	60.7	9.2	76.5	-52.1	8

Table 4.2. Directions obtained from both thermal and AF demagnetization for sites with $\alpha_{95} < 10°$ and the corresponding latitude and longitude of the VGP. The number of rejected samples by the Vandamme cut-off is given between brackets.

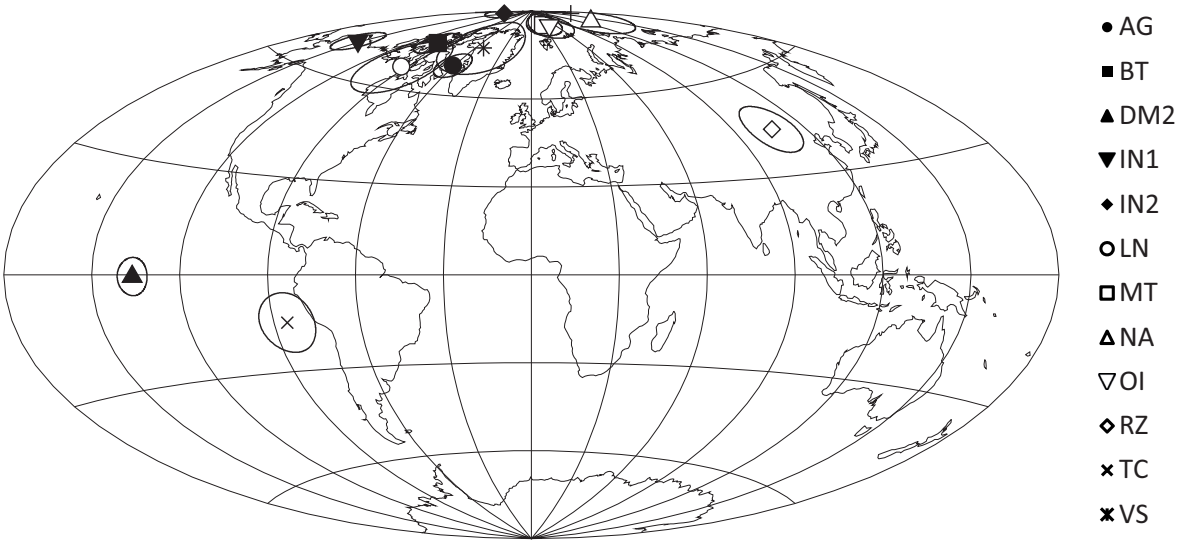

Fig. 4.8. Locations of the VGPs including the α_{95} intervals. Sites DM2 and TC indicate an excursion with a VGP around the equator in the Pacific Ocean and near South America respectively. Site RZ might also indicate an excursion with a VGP in China.

excursion. The poles of sites DM2 and TC are near the equator, which clearly indicates an excursion. However, it should be noted that some outcrops were slightly tilted and consequently their orientations are less reliable.

4.3. Anhysteretic remanent magnetization (ARM) test

Based on the results of the rock-magnetic analyses and the demagnetization, a subset of the sites was subjected to the ARM-test in order to obtain the best set temperature for the MSP experiments. The sites from group H that did not easily lose their NRM in both the thermal and AF demagnetization and showed uniform behavior (AG, IN2, MT, NA, and OI; from now on called group I) were by all means part of these subset. They also generally showed the least change in directional behavior and traces of overprints. On the other hand, sites from group L (BT, DM1, and RZ) and sites from group M with a comparable low dominant Curie temperature (TC) lose their susceptibility and magnetization so quickly that it is not meaningful to execute any MSP experiments and therefore ARM-test.

The other sites have to be assessed individually. Besides the quick demagnetization that is already

Site	T_1 (°C)	T_2 (°C)	T_{set} (°C)
AG	240	360	240
CS	240	360	240
IN1	240	360	240
IN2	360	450	360
LN	240	360	-
MC	240	-	-
MT	360	450	360
NA	360	450	360
OI	360	450	360

Table 4.3. Test temperatures for the ARM-test and the chosen set temperature for the MSP experiments.

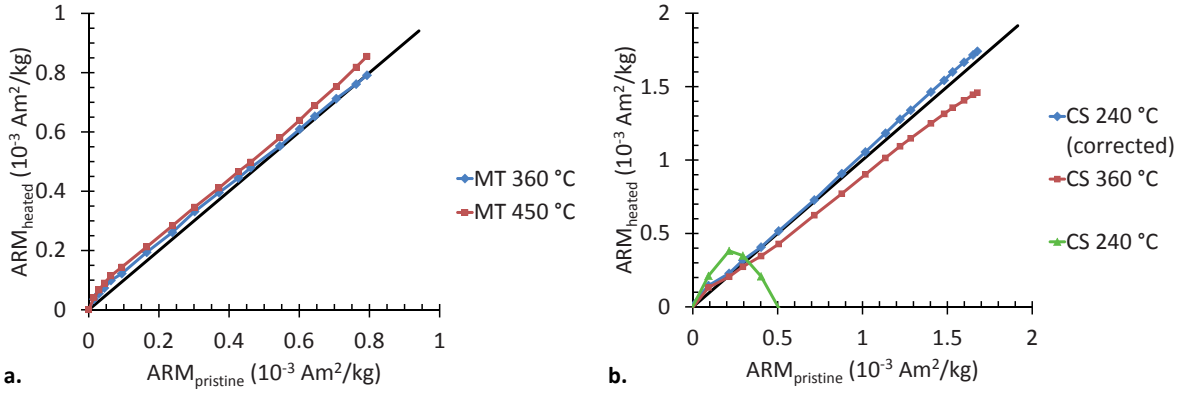

Fig. 4.9. ARM-test diagrams for two sites. Site MT (**a.**) shows good behavior as the data points are near the diagonal. For 360 °C specimens only acquire slightly more ARM at low AF strengths, for 450 °C over the whole range of AF strengths. Therefore, 360 °C is chosen as set temperature for the MSP experiments. For site CS (**b.**) the data of 240 °C is corrected as desribed in the text. Specimens that are heated to 240 °C show more desirable behavior so it is chosen as set temperature for the MSP experiments.

mentioned, large overprints and within-site variation are main conditions to exclude sites. As these both occur for sites DM2 and VS, these sites are not subjected to the ARM-test. Sites CS, IN1, LN, and MC may be suspect for overprints, variation and alteration, but these sites are subjected to the ARM-test because they can easily be measured in the same group as the aforementioned sites on the robotized SQUID magnetometer.

As the alteration temperature can only be determined with an accuracy of 50 - 100 °C and the 'real' alteration temperature is generally a little higher than the values mentioned in table 4.1, somewhat higher temperatures were used in the ARM-test: 240, 360, and 450 °C (table 4.3). Most sites from group I (IN2, MT, NA, and OI) were tested at the higher two temperatures, the other sites (AG, CS, IN1, LN, and MC) at the lower two. Site MC was only tested at 240 °C since not enough material was available to test it at two temperatures. In some cases we chose to do an ARM-test at a temperature above the alteration temperature, because ideally too little of the NRM is demagnetized at the alteration temperature for a good MSP experiment. This was only done when the alteration at this temperature was slightly higher than the restriction of 5%.

From the resulting ARM acquisition curves (figures A3.1-9), it can be seen that sites of group I show the best behavior as they most nearly approach the diagonal y = x (e.g. figure 4.9a). Sites LN and MC showed such devious behavior that is was not meaningful to subject them to a MSP experiment. Site IN1 was a questionable case, but since the data approaches the diagonal for higher field strengths, it

was decided to pick up IN1 in the MSP experiments.

At first hand, site CS showed abnormal behavior (figure 4.9b). The ARM signal for the samples that are heated to 240 °C quickly dives down below zero, while the samples that are heated to 360 °C show a line quite near to the diagonal. The reason this happens in the ARM acquisition curve is the scale factor b (De Groot, Dekkers, et al., 2012). This factor is defined as the square root of the ratio of the 0-μT-series' and 35-μT-series' NRM. Since the NRM of the samples that are heated to 240 °C in the direction of the ARM is close to zero (some below and some above), the series are not scaled properly. When this scale factor b is corrected to the value of the samples that are heated to 360 °C (0.93), more expected behavior is shown. The correction of b seems reasonable, since the difference between scale factors of two temperatures for one site is generally small (< 0.1) and this b is close to 1 as it should be.

For all accepted sites the lowest temperature was chosen as set temperature for the MSP experiments (table 4.3). It is trivial that a lower temperature shows more ideal behavior in the ARM acquisition curves as less should be changed inside the sample. However, the difference between the lower and higher temperature curves was generally too high to try a higher temperature despite of the fact that in some cases only little of the NRM was demagnetized at this temperature. For one site (OI) there was hardly any difference between the two temperatures. The only site that shows better behavior for the higher temperature was IN2, but because of the relatively short core from which the specimens were cut, the heated series only consisted of two specimens. These specimens showed slightly divergent behavior at 360 °C, so they are less reliable and for site IN2 the lower temperature was chosen as set temperature.

4.4. Paleointensity determination

4.4.1. Thellier-Thellier method

Based on the criteria as mentioned for the ARM acquisition, the same sites were subjected to the Thellier paleointensity experiments. Site BT was despite of its low Curie temperature added to this set because it shows quite good Zijderveld diagrams and does not lose its NRM during demagnetization as quick as other sites from group L. The same temperature subdivision into two groups was made as for the MSP experiments: a lower temperature group (AG, BT, CS, IN1, LN, and MC) with temperature intervals of 40 °C (80 - 480 °C) and a higher temperature group (IN2, MT, NA, and OI) with intervals of 50 °C (100 - 600 °C).

Of the 49 specimens subjected to the Thellier method, 32 passed the PICRIT-03 and/or SELCRIT-1 criteria (table 4.4, figures A4.1-33). 18 specimens from group I passed the stricter PICRIT-03 criteria. One specimen of site IN2 only passed the SELCRIT-1 criteria, while one specimen of site OI did not pass both selection criteria. Because only one data point of this specimen really deviated in the middle of the linear segment and therefore only β fell out of the selection criteria, it was included in the results. Of the other 13 specimens that passed one of the criteria sets, only one specimen of site CS and all four specimens of site MC passed the stricter PICRIT-03 criteria.

For sites CS, IN1, and LN only one or two out of five specimen passed the criteria. CS shows two totally different values for the paleointensity as it uses two totally different temperature intervals for the linear fit (figures 4.10a-b), so these values are not reliable. Furthermore, sagging and/or the removal of an overprint is clearly visible and the extra criterion of $\delta t^* < 5$ is not met. The same is true for sites

Site	PI (μT)	σ (μT)	T_{min} (°C)	T_{max} (°C)	N	β	f	q	α (°)	MAD (°)	DRAT (%)	δt*	Class
AG-2B	35.6	2.3	120	400	8	0.07	0.22	2.8	0.8	2.2	8.1	14.3	B
AG-9B	35.6	2.4	80	360	8	0.07	0.38	4.9	0.8	1.6	9.1	10.0	B
AG-11A	35.3	2.3	20	360	9	0.06	0.40	5.4	4.0	1.9	8.3	8.3	B
AG-12B	32.9	2.3	20	400	10	0.07	0.47	5.8	2.9	2.0	8.9	12.6	B
CS-4B	27.6	2.6	160	360	6	0.09	0.37	3.1	10.1	7.1	8.2	20.8	B
CS-6B	204.8	11.6	20	160	4	0.06	0.47	5.4	3.0	2.6	0.4	17.4	A
IN1-12B	37.7	3.7	20	240	6	0.10	0.53	4.1	10.5	5.1	9.9	13.4	B
IN2-2A	80.1	5.5	20	500	10	0.07	0.53	6.4	3.5	2.2	4.7	0.8	A
IN2-4C	76.6	5.8	20	500	10	0.08	0.43	4.7	3.9	2.2	8.8	0.6	B
IN2-5C	74.9	6.4	20	500	10	0.08	0.40	3.8	2.2	1.7	6.1	1.1	A
IN2-7B	72.1	5.0	20	450	9	0.07	0.36	3.9	3.4	2.0	6.4	1.4	A
IN2-8B	77.7	5.4	20	500	10	0.07	0.42	5.0	4.0	1.7	3.9	1.0	A
LN-4B	74.3	5.5	20	480	12	0.07	0.93	10.8	4.5	4.4	9.5	18.3	B
LN-7B	88.6	7.8	20	480	12	0.09	0.97	9.6	4.1	3.5	9.2	15.0	B
MC-3D	28.8	2.8	20	280	7	0.10	0.52	4.4	4.5	2.3	6.6	8.2	A
MC-5A	30.0	2.3	20	320	8	0.08	0.82	8.8	2.4	3.0	6.3	7.5	A
MC-6A	33.5	2.5	20	320	8	0.07	0.79	8.5	0.1	1.6	2.7	8.2	A
MC-9B	28.3	2.3	20	400	10	0.08	0.86	9.3	2.7	3.4	6.8	7.6	A
MT-6C	47.5	3.2	20	500	10	0.07	0.47	5.8	4.3	2.0	6.8	1.2	A
MT-7B	49.8	4.5	20	500	10	0.09	0.47	4.1	2.8	2.2	2.8	1.4	A
MT-9A	46.9	3.8	20	500	10	0.08	0.48	4.7	3.9	2.0	2.5	1.8	A
MT-11C	47.2	4.0	20	500	10	0.08	0.49	4.7	3.9	1.6	5.3	1.1	A
MT-15B	48.8	3.6	20	500	10	0.07	0.52	5.8	4.9	2.5	5.3	2.9	A
NA-2B	38.3	2.5	20	500	10	0.06	0.58	7.4	4.3	3.1	3.1	3.4	A
NA-4B	40.4	2.9	20	500	10	0.07	0.58	6.6	2.4	2.2	3.4	2.4	A
NA-5B	41.0	2.9	20	500	10	0.07	0.61	7.0	6.0	3.0	2.9	2.8	A
NA-6B	44.6	2.8	20	500	10	0.06	0.59	7.6	3.1	1.8	4.1	3.3	A
NA-11B	38.1	2.0	20	500	10	0.05	0.59	9.0	3.7	1.9	2.9	2.0	A
OI-3B	121.7	8.7	20	500	10	0.07	0.56	6.5	0.9	1.3	2.3	1.3	A
OI-5C	132.6	12.5	20	500	10	0.09	0.57	4.9	4.0	1.8	2.8	1.6	A
OI-8C	121.5	6.6	100	500	9	0.05	0.51	7.5	2.7	1.4	3.5	1.6	A
OI-9A	121.6	8.1	20	500	10	0.07	0.56	7.0	0.8	1.0	2.6	2.3	A
OI-11B	114.1	13.7	20	500	10	0.12	0.56	3.7	1.9	1.3	5.8	5.3	C

Site	PI (μT)	σ (μT)	n (rejected)
AG	34.8	2.3	4 (1)
IN2	76.3	5.6	5
MC	30.2	2.5	4
MT	48.0	3.8	5
NA	40.5	2.6	5
OI	122.3	10.3	5

Table 4.5. Average Thellier-Thellier paleointensities (PI) per site with one standard deviation σ, based on n specimens.

IN1 and LN, for which also the pTRM checks are bad. When the temperature interval is reduced to the segment with fairly good checks, other criteria are not met anymore. In short, these sites are not suited for the Thellier method and the results are not taken into account.

The other six sites showed quite homogeneous behavior so the average of their samples is calculated (table 4.5). It should be noted that for sites AG and MC the values of δt* are rather high (> 7.5). However, the individual results are in good agreement and pTRM checks are sometimes reasonably good so they are taken into account for any potential comparison with the other paleointensity methods. This results in a paleointensity of 30.2 ± 2.5 μT for site MC and 34.8 ± 2.3 μT for site AG, where one of the five specimens was omitted.

Group I clearly shows the best results. Except for site AG and two other specimens, all sites pass the PICRIT-03 criteria and the individual results are in good agreement with each other. Furthermore, values of δt* are except for one specimen all well below our threshold of 5. For some specimens even the full temperature range would pass the criteria, but from 500 °C onwards data points are further removed from the linear fit through the other data. In these cases, the upper temperature limit is manually adjusted to 500 °C. Although some specimens might still pass the criteria with the full temperature range, most values are better with an upper limit of 500 °C. ThellierTool automatically takes the largest temperature interval that meets the set of criteria as it maximizes q (Leonhardt et al., 2004), which is strongly dependent on the fraction of NRM f (Coe et al., 1978).

Site IN2 (figure 4.10c) shows a quite high average for the paleointensity of 76.3 ± 5.6 μT. The pTRM checks are good in the chosen temperature interval and it has the lowest values for δt* of all sites, but the fraction of NRM that is demagnetized is relatively small. For MT (figure 4.10d) a paleointensity of 48.0 ± 3.8 μT is found. Here a slight zig-zag behavior is visible, which is characteristic for the effect of pTRM tails in the IZZI protocol (Tauxe, 2010). Together with site NA (figure 4.10e), with a value of 40.5 ± 2.6 μT, these sites most resemble the current intensity of the Earth's magnetic field at Mt. Etna of 45.0 μT. Good pTRM checks can be seen here as well, with the linear fit almost exactly through the original NRM. Finally, site OI (figure 4.10f) shows by far the largest paleointensity: 122.3 ± 10.3 μT.

Table 4.4. Individual results from the Thellier-Thellier method of all specimens that passed at least one of the sets of selection criteria. The obtained paleointensity (PI) per specimen is displayed, including one standard deviation σ. This paleointensity is based on a linear fit between T_{min} and T_{max} through N data points. Furthermore, the standard deviation divided by the slope of the linear fit β, the fraction of NRM f, the quality factor q, the angular difference between anchored and not-anchored solution α, the maximum angular deviation MAD, and the deviation of the pTRM check from its corresponding pTRM normalized to the length of the segment DRAT are given. All specimens met either the PICRIT-03 (Class B) or SELCRIT-1 (Class A) selection criteria, except for specimen OI-11B (Class C) that nevertheless was included in the results (see text).

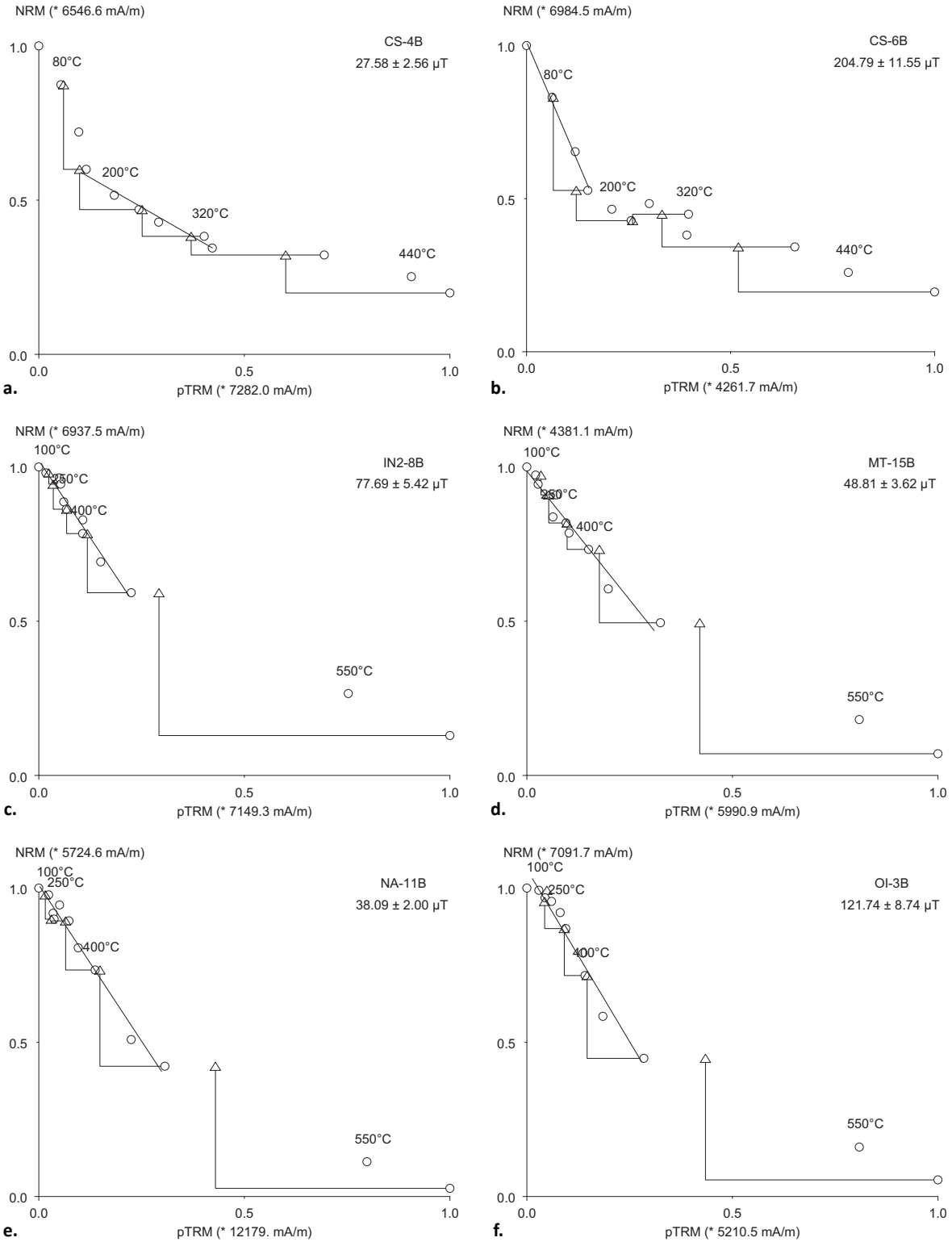

Fig. 4.10. Representative Arai diagrams for several sites. For site CS (**a.** and **b.**) only two specimens pass one of the sets of selection criteria but they yield two totally different values for the paleointensity as it uses two totally different temperature intervals for the linear fit. Furthermore, sagging and/or the removal of an overprint is clearly visible so the results are not reliable. Sites IN2 (**c.**), MT (**d.**), NA (**e.**), and OI (**f.**) show the best behavior. The paleointensity is determined over a large range of temperatures up to 500 °C and pTRM checks are generally good. Data points for temperatures > 500 °C deviate from the linear fit but have shown alteration in the susceptibility curves for this temperature. For site MT a slight zig-zag behavior is visible, which is characteristic for the effect of pTRM tails in the IZZI protocol.

Site	PI (μT)	CI (μT)	n (rej.)	r^2	a	b	ΔDSC (μT)	ε_{alt} (%)
MSP-DB								
AG	33.3	24.5 - 40.3	12	0.843	0.0071	0.237	-	-
CS	103.7	88.1 - 131.6	11 (1)	0.861	0.0047	0.486	-	-
IN1	32.2	28.5 - 35.4	12	0.964	0.0162	0.523	-	-
IN2	43.8	42.1 - 45.5	12	0.986	0.0033	0.145	-	-
MT	34.4	33.0 - 35.8	11 (1)	0.994	0.0051	0.177	-	-
NA	30.9	27.5 - 33.9	13	0.967	0.0075	0.232	-	-
OI	66.5	63.2 - 70.3	13	0.964	0.0031	0.209	-	-
MSP-DSC								
AG	28.3	25.6 - 30.7	12	0.982	0.0487	1.377	-5.0	2 - 6
CS	84.0	75.3 - 96.6	11 (1)	0.925	0.0111	0.928	-19.8	8 - 14
IN1	27.2	19.7 - 33.0	12	0.902	0.0540	1.469	-5.0	7 - 12
IN2	34.5	31.7 - 37.0	12	0.975	0.0346	1.193	-9.3	2 - 6
MT	26.6	21.3 - 31.0	11 (1)	0.947	0.0636	1.694	-7.8	3 - 7
NA	24.6	19.1 - 28.9	12 (1)	0.939	0.0886	2.177	-6.3	4 - 9
OI	52.9	50.7 - 55.3	12 (1)	0.977	0.0197	1.043	-13.6	5 - 7

Table 4.6. Results obtained from the MSP experiments by using both the DB and DSC protocol. Paleointensities (PI) are displayed with the corresponding confidence interval (CI), based on n specimens. Furthermore, the parameters r^2, a, and b are given for the linear fit through the data points. In case of the DSC protocol, the correction with respect to the DB results and the relative alteration error are given. Generally high values for r^2 are obtained, although some data points were rejected. A strong negative correction can be seen for the DSC protocol, as well as high values for the relative alteration error.

4.4.2. Multispecimen method

Most sites that were subjected to the MSP method (table 4.3), yielded technically good results (table 4.6, figures A5.1-7). Only sites AG and CS yielded r^2 values for the linear fit of the MSP-DB experiments < 0.90. The other sites showed r^2 values well above 0.95 for the MSP-DB protocol and all sites yielded a $r^2 > 0.90$ for the MSP-DSC protocol. However, values for the relative alteration error ε_{alt} were rather high. They range between 2% and 9% for sites of group I and between 7% and 14% for the other sites, whereas maximally 3% is preferred. Values depend on the specific site and the applied field strength.

Some sites show maximally one data point that varies more than twice the confidence interval including all data. These data points were rejected and both the linear fit and uncertainty envelope were calculated again. Furthermore, corrections by the MSP-DSC experiments are all negative and quite large, between -5.0 and -19.8 μT. Higher paleointensities in the DB protocol are generally more strongly corrected.

Site AG yields a paleointensity of 33.3 μT [24.5 - 40.3 μT] (intersection of uncertainty envelope with the x-axis (confidence interval) is given between brackets) for the DB protocol (figure 4.11a) compared to 28.3 μT [25.6 - 30.7 μT] for the DSC protocol (figure 4.11b). The MSP-DSC method clearly reduces the confidence interval. Even the data at 80 μT nicely fit the data at lower field strength, although some scatter occurred in the MSP-DB plot which lead to a wide uncertainty envelope. The paleointensity for the MSP-DB experiment, however, is hardly affected by this scatter.

Site CS yields high paleointensities of 103.7 μT [88.1 - 131.6 μT] for the DB protocol and 84.0 μT [75.3 - 96.6 μT] for the DSC protocol with large confidence intervals, since the measured data are all below the determined paleointensities. Higher field steps were not carried out, because the linearity of magnetization with applied field is uncertain above 100 μT (Fabian and Leonhardt, 2010) and the other sites in the group (AG and IN1) yielded much lower paleointensities. For both protocols, quite some scatter occurs around the confidence interval at lower field strengths. Alteration is clear during the DSC

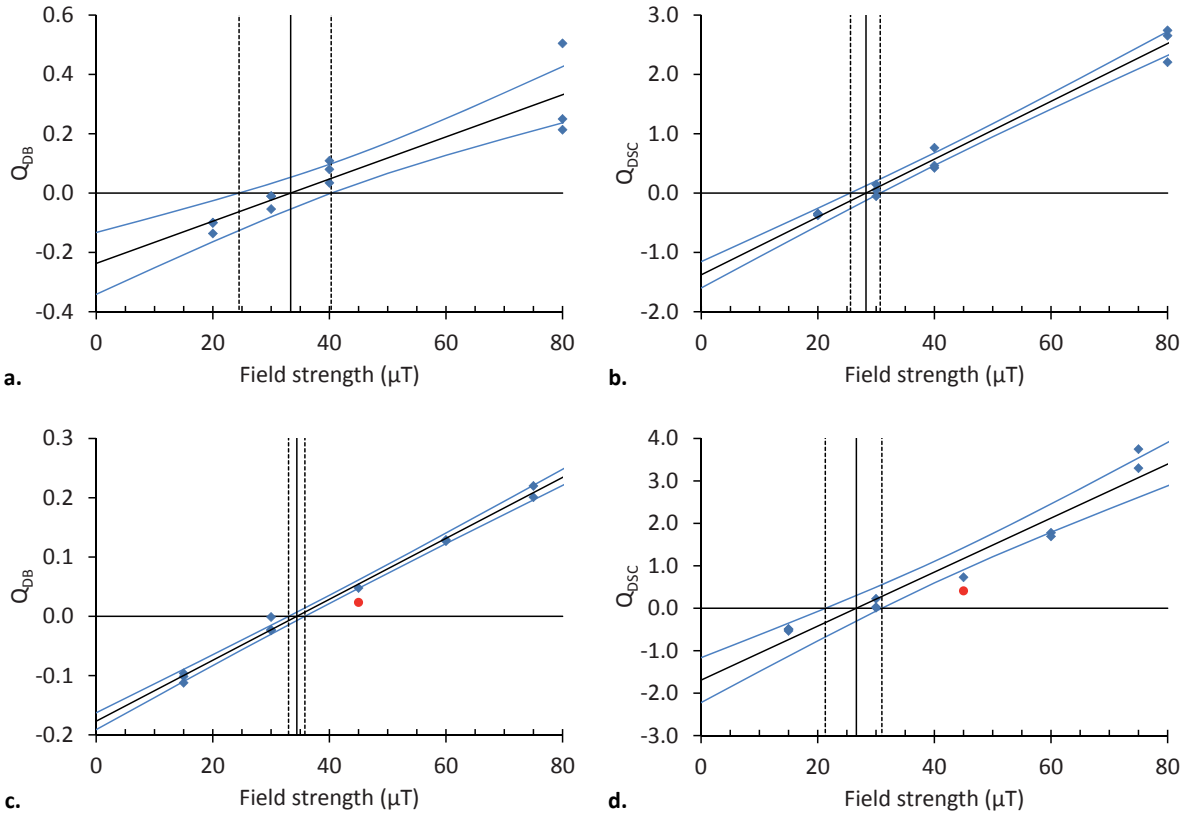

Fig. 4.11. Both DB and DSC MSP plots for two sites. Site AG (**a.** and **b.**) shows a large confidence interval and quite some scatter at 80 μT for the DB protocol. After correction by the DSC protocol the confidence interval and the scatter have decreased. The opposite occurs for site MT (**c.** and **d.**). For both protocols one data point is rejected (red dots) and a slight curvature of data points can be seen in the DSC plot.

steps as ε_{alt} is very high with values up to 14%.

The last site of the low temperature group, IN1, clearly shows technically better results for the DB protocol: 32.2 μT [28.5 - 35.4 μT]. Increased scatter at 80 μT for the DSC protocol leads to a larger confidence interval and r^2 value in the DSC experiments (27.2 μT [19.7 - 33.0 μT]), but the paleointensity was hardly affected if the data at 80 μT would be omitted. However, alteration is considerable for this site with values up to 12% for ε_{alt}.

Data for site IN2 is nicely distributed around the estimated paleointensity for the DB protocol, yielding values of 43.8 μT [42.1 - 45.5 μT]. This value is corrected to 34.5 μT [31.7 - 37.0 μT] by the DSC protocol. Site MT yields the highest r^2 and the smallest confidence interval in the MSP-DB experiments (0.994), although it should be noted that one data point was omitted. The paleointensities are 34.4 μT [33.0 - 35.8 μT] for the DB protocol (figure 4.11c) and 26.6 μT [21.3 - 31.0 μT] for the DSC protocol (figure 4.11d). In the DSC plot it is notable that the data points seem to be curved: low and high field strengths are plotted above the linear fit, intermediate field strengths (including the omitted data point) are plotted below the linear fit. The confidence interval is strongly increased by the DSC correction.

Some scatter occurs in the DB plot for site NA, but it is evenly distributed above and below the linear fit, yielding a paleointensity of 30.9 μT [27.5 - 33.9 μT]. After correction by the DSC protocol (24.6 μT [19.1 - 28.9 μT]) a similar curve is visible as for site MT and one data point is omitted. The highest paleointensity is again found for site OI, 66.5 μT [63.2 - 70.3 μT] for the DB protocol and 52.9 [50.7 - 55.3 μT] for the DSC protocol. One data point at 75 μT is omitted as it deviates from the others.

Site	PI (μT)	σ_{PI} (μT)	pTh-slope	σ_{pTh}	range (mT)	r^2	$B_{1/2}$ (mT)	$\sigma_{B1/2}$ (mT)	n
AG	23.1	0.9	1.32	0.14	7.5 - 80	1.000	30.2	2.0	6
CS	17.0	0.2	0.37	0.04	15 - 100	0.984	23.1	1.6	6
DM1	24.0	0.4	1.44	0.07	10 - 100	0.992	24.1	2.6	6
IN2	34.0	2.2	3.00	0.34	2.5 - 40	0.997	49.1	3.3	6
MT	26.4	0.3	1.82	0.04	2.5 - 100	0.996	39.5	0.8	6
NA	23.0	0.1	1.29	0.01	5 - 100	0.993	33.2	0.3	6
OI	34.1	0.3	3.02	0.05	2.5 - 100	0.997	42.1	0.9	6
VS	22.1	0.5	1.15	0.08	20 - 100	1.000	38.6	0.7	5

Table 4.7. Results from the pseudo-Thellier method. Based on the average pTh-slope of n specimens and its standard deviation σ_{pTh} the paleointensity (PI) and the related standard deviation are calculated. The pTh-slope is determined by a linear fit with coefficient of determination r^2 over a range of AF strengths. Furthermore, $B_{1/2}$ and its uncertainty are obtained.

4.4.3. Pseudo-Thellier method

The pTh-slope was assessed for all 15 sites. However, the check of $B_{1/2}$ excluded some sites from a paleointensity determination with the pseudo-Thellier method. Sites BT, IN1, LN, MC, RZ, and TC yielded too low values with $B_{1/2}$ < 23 mT and clearly showed non-ideal behavior. Site DM2 yielded a value slightly above 23 mT but the behavior of several samples was so divergent that the site was also discarded for paleointensity determination. For the eight remaining sites (table 4.7) the linear part in the AF-ARM versus AF-NRM diagrams (figures A6.1b-8b) was used to determine the range of field strengths over which the pTh-slopes in the ARM Arai diagrams (figures A6.1a-8a) were calculated.

Site AG yielded a pTh-slope of 1.32 ± 0.14, resulting in a paleointensity of 23.1 ± 0.9 μT. Variation occurred in the mass normalized NRM, resulting in some scatter in the pTh-slope. However, results for all specimens fell within twice the standard deviation so no specimens were omitted. Despite of the scatter in the mass normalized NRM, the Arai diagram for all specimens was almost perfectly linear, resulting in a r^2 of 1.000.

For site CS a quite low paleointensity is obtained: 17.0 ± 0.2 μT. A large overprint has to be removed in the original NRM, explaining the range for the pTh-slope only to start at 15 mT and the r^2 of the slope to be lower than for other sites. $B_{1/2}$ is at the lower boundary of acceptation. The same is true for site DM1, which resulted in a paleointensity of 24.0 ± 0.4 μT.

Some notable behavior can be seen for site IN2 (figures 4.12a-b). A little scatter occurs in the mass normalized NRM, but especially the ARM acquisition is remarkable. Besides the difference between specimens, a clear change in behavior can be seen at intermediate field strengths which is not equally strong for every specimen. Specimens with a lower original NRM generally acquire more ARM. Only the low AF part of the Arai diagram is used for the determination of the pTh-slope, since the specimens behave similarly in this region. This results in a paleointensity of 34.0 ± 2.2 μT.

Sites MT, NA, and OI (figures 4.12c-d) showed the most ideal behavior as both $B_{1/2}$ and the pTh-slope could be determined with a low uncertainty and almost the full range of field strengths is used to determine this slope. However, it should be noted that for sites MT and OI the ARM acquisition is not yet fully saturated at 150 mT. This can clearly be seen in the Arai diagram but also in the the AF-ARM versus AF-NRM diagram where the linear fit would not go through the origin. Further ARM acquisition would only slightly increase $B_{1/2}$ but not change the obtained paleointensities. The resulting paleointensities are 26.4 ± 0.3 μT for site MT, 23.0 ± 0.1 μT for site NA, and 34.1 ± 0.3 μT for site OI.

Site VS shows an overprint in the Arai diagram that was already seen in the AF demagnetization. For

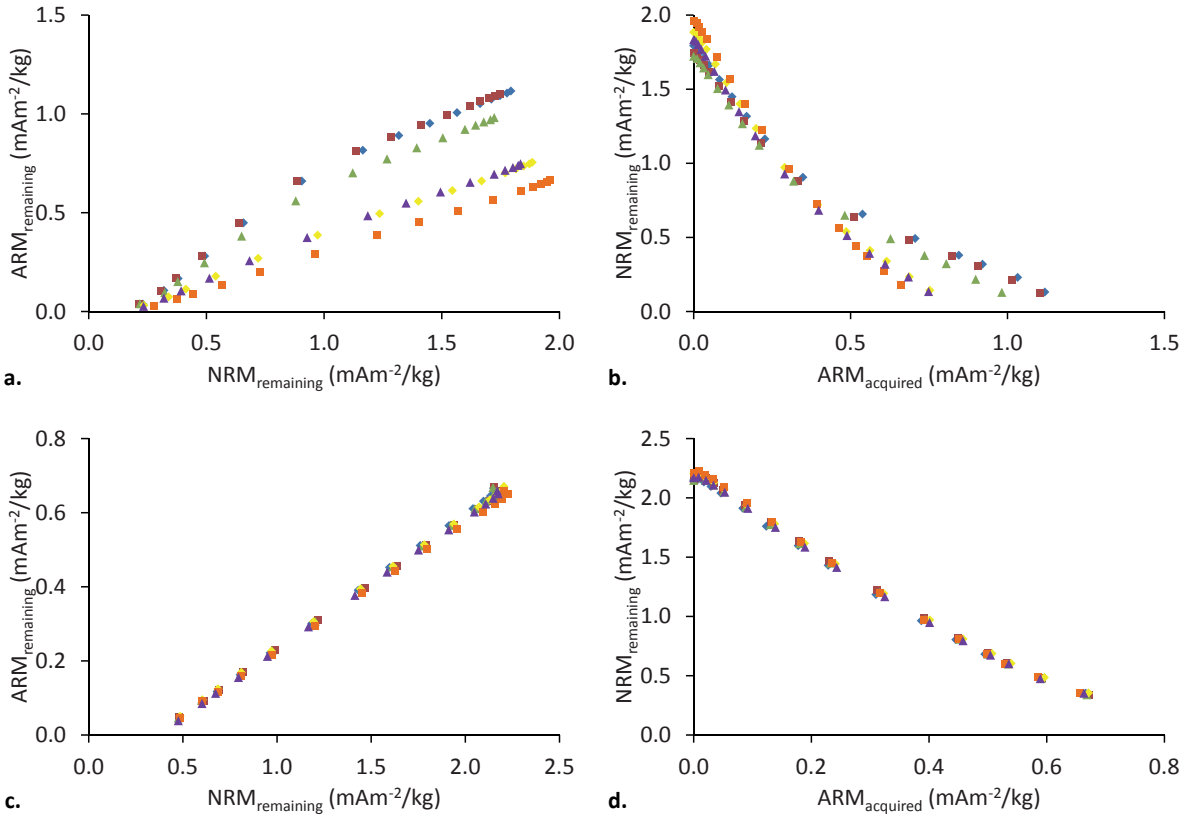

Fig. 4.12. AF-ARM versus AF-NRM diagrams (**a.** and **c.**) and ARM Arai diagrams (**b.** and **d.**) for two sites. Site IN2 shows remarkable behavior as a change in behavior occurs at intermediate field strengths (**a.**). Only the low AF part of the Arai diagram (**b.**) is used for the determination of the pTh-slope, since the specimens behave similarly in this region. Better behavior is shown by site OI. Hardly any overprint can be seen in the Arai diagram (**d.**) and the magnetization seems to be carried by the same magnetic grains after ARM acquisition (**c.**), so almost the full range of AF strengths can be used to determine the pTh-slope.

higher field strengths it shows more linear behavior, although there is a large variation in the acquired ARM. This leads to some scatter in the pTh-slope but all values are well within twice the standard deviation, yielding a paleointensity of 22.1 ± 0.5 µT.

4.4.4. Comparison

When the obtained paleointensities from all methods are compared (table 4.8), we see major differences. Whenever a comparison with the other methods is available, Thellier always yields the highest value. For site OI the Thellier method even results in a paleointensity two to four times as high as for the other methods. For site AG however, the Thellier method yields a comparable value to the MSP-DB method.

As discussed before, the MSP-DSC method corrects all values of the MSP-DB method downwards. Furthermore, the pseudo-Thellier method yields the lowest paleointensity for all sites that can be compared. However, values of sites IN2, MT, and NA are comparable to the results of MSP-DSC within the uncertainty range. Finally, site CS is remarkable as results of the MSP methods differ largely from the pseudo-Thellier method.

Site	Age (ka)	Thellier PI (μT)	MSP-DB PI (μT)	MSP-DSC PI (μT)	pseudo-Thellier PI (μT)
AG	154.9	34.8	33.3	28.3	23.1
CS	41.3	-	103.7	84.0	17.0
DM1	32.9	-	-	-	24.0
IN1	132.6	-	32.2	27.2	-
IN2	-	76.3	43.8	34.5	34.0
MC	28.7	30.2	-	-	-
MT	126.4	48.0	34.4	26.6	26.4
NA	111.9	40.5	30.9	24.6	23.0
OI	28.6	122.3	66.5	52.9	34.1
VS	121.2	-	-	-	22.1

Table 4.8. Summary of the paleointensity results that are obtained from the four different methods. For all sites Thellier-Thellier yields the highest value, followed by MSP-DB, MSP-DSC, and pseudo-Thellier.

5. Discussion

In this study, five out of fifteen sites (group I) could be subjected to all paleointensity methods. The selection criteria are discussed because these sites showed the best behavior in the preliminary rock-magnetic analyses, demagnetization, and ARM-test. The paleointensity methods are compared and possible sources of error are mentioned to explain the differences between the methods and to seek for a restriction on the varying results. Furthermore, the obtained directions are discussed to see whether an excursion might have occurred during the formation of the regarding site.

5.1. Directions

The obtained paleodirections were generally near the present day orientation of the Earth's magnetic field as expected, but some sites showed clearly deviating directions, which could suggest an excursion of the magnetic field (table 4.2, figure 4.8). Sites DM2 and TC deviate most, as they have negative inclinations and a VGP around the equator. Site DM2 might be of particular interest as it should be older than site DM1 (32.9 ± 10.6 ka), which is near the age of the Laschamp excursion of 40.70 ± 0.95 ka (Singer et al., 2009). Site TC (145.8 ± 14.0 ka) is about 25 ka too old for the Blake excursion that occurred approximately 115 - 120 ka (Tric et al., 1991; Fang et al., 1997).

The VGP for site DM2 is at latitude -0.6° and longitude 223.7°, with the remark that the outcrop was probably slightly tilted. The direction is between those from the Laschamp, Olby, and Louchadière flows, especially for the longitude. These yield varying values between -53.5° and 13.2° latitude and 49.8° - 272.2° longitude (Roperch et al., 1988; Chauvin et al., 1989; Guillou et al., 2004). However, values for longitude yield almost opposite values so any longitude could fit. Values agree better with VGPs for the Laschamp excursion that are found on Iceland with latitude -6.5° and longitude 251.9° (Ferk and Leonhardt, 2009; Vérard et al., 2012). Especially with this latitude the magnetization could correspond to a transitional VGP (Singer et al., 2009). Unfortunately, no paleointensity could be obtained for sites DM2 and TC to further substantiate a possible excursion as indicated by the directions.

The direction of site RZ also deviates from the present orientation but with a positive latitude of about 44.1°. Again the lack of a paleointensity determination could not clarify whether really an excursion occurred during the magnetization of this lava flow. The age is determined with a rather large uncertainty (30.8 ± 21.2 ka), so a correlation with the Laschamp excursion may be suggested. Lastly, site IN1 shows a quite low latitude of 69.1° but the sampling site was cracked in such a way that the orientation could not be determined with certainty. The age of 132.6 ka and the rather low obtained paleointensity by the MSP-DB method (32.2 μT), however, might relate it to the Blake excursion.

Based on the age and deviating directions, sites DM2 and RZ may tentatively be attributed to the Laschamp excursion. Sites IN1 and TC have an age that is near that of the Blake excursion but are both slightly too old for a good fit. Except for site IN1, paleointensity determinations for these sites unfortunately were not possible to confirm whether an excursion might be recorded. Furthermore, it may be possible that the orientation of the rock at some sites has changed since it was magnetized, as the outcrops could be slightly tilted. We have good control about the age of the sites since they were sampled according to the published UTM coordinates and in collaboration with the same geologist that did the fieldwork for the dated samples.

5.2. Selection criteria

Five out of fifteen sites (group I) could be subjected to all paleointensity methods. We selected these sites of group I based on several preliminary measurements. However, one or more of the other sites could show good behavior in one of the preliminary measurements, indicating that one of these measurements on itself is not sufficient to distinguish between suitable and non-suitable samples.

A first important categorization was made based on the magnetic susceptibility curve, which reveals chemical alteration. All sites of group I were part of group H (high alteration temperatures and Curie temperatures) so the criterion of > 80% of susceptibility left at 400 °C is appropriate to make a first selection. None of the sites of group L and M (< 80% of susceptibility left at 400 °C) were part of group I and just two sites could be subjected to one of the paleointensity methods. However, not all sites of group H were suitable for paleointensity determination so further measurements are required. Sites of group H trend to be more SD in a Day plot but the suitable sites cannot be discriminated from the non-suitable sites of this group, indicating grain size is not the only important parameter for a site to be suitable for paleointensity determination.

Both thermal and AF demagnetization are needed to account for overprints and homogeneity. In the NRM decay curves the susceptibility behavior is largely reflected as sites from group H generally stay more strongly magnetized up to higher temperatures and field strengths. Sites of group I all show a more convex shape when the demagnetization is plotted against temperature. Furthermore, homogeneity can be assessed by checking if all specimens demagnetize similarly. From the Zijderveld diagrams we observe that all sites of group I have minor overprints in thermal demagnetization and hardly any in AF demagnetization. Furthermore, the magnetization decays in a straight line through the origin. All the other sites show either large overprints, a decay not through the origin, or both. This turns out to be a second criterion to select suitable specimens in addition to susceptibility criterion mentioned above. The behavior in the Zijderveld diagrams is reflected in the NRM decay curves.

Finally, the ARM-test is used to assess the suitability of samples for the MSP experiments. Again all sites of group I pass this test, indicating that there is little change of ARM capacity after heating to the set temperature for MSP experiments. Two more sites passed the ARM-test but these sites could have been excluded in an earlier stage based on the rock-magnetic analyses and demagnetization. The ARM-test was designed as a test for the MSP method by De Groot et al. (2012) as it is able to visualize small changes in the magnetic state of specimens, either caused by chemical or magnetic alteration. This information can be used for all thermal paleointensity methods.

We conclude that several preliminary measurements are needed to make a selection of suitable specimens for paleointensity determination. The first selection is done by the magnetic susceptibility curve, where > 80% should be remaining at 400 °C. These sites generally show more SD behavior, but no conclusions can be drawn based on the Day plot. Both thermal and AF demagnetization supply the necessary extra information. Zijderveld diagrams should be checked for (large) overprints and a decay that does not go through the origin, which is also reflected in the NRM decay curves. Finally, the ARM-test gives information about small changes in the magnetic state of specimens, thereby explaining possible alterations that would not be expected based on the other preliminary measurements.

5.3. Paleointensity determination

The methods that are used to determine the paleointensity in this study yield varying results. Sites

of group I are available to compare the different methods (table 4.8). For all of these sites, the Thellier method yields the highest outcome, followed by the MPS-DB results which are corrected to even lower values by the MSP-DSC protocol. The relative pseudo-Thellier method yields the lowest paleointensities for all sites. Results of each method will be discussed and we attempt to find an explanation for these discrepancies.

5.3.1. Thellier-Thellier method

The Thellier method generally yielded values that are closest to the present day IGRF reference value of 45.0 μT. None of the sites really indicates an excursion since the lowest obtained paleointensity is 30.2 ± 2.5 μT for site MC. Based on the directions an excursion was not expected for the sites that were subjected to the Thellier method, although site MC could not be properly oriented. Sites IN2 (76.3 ± 5.6 μT) and OI (122.3 ± 10.3 μT) clearly stand out with high intensities.

Only the upper (steeper) part of the Arai diagrams for these sites is used for paleointensity determination. Although good linear behavior is shown over a broad range of temperatures (20 - 500 °C) for both sites, the fraction f that is demagnetized is only ~0.5. This means that the other 50% is demagnetized in a small range of temperatures (500 - 600 °C). Using the whole range would lead to a shallower slope and a lower paleointensity. However, this part is above the alteration temperature of 325 - 425 °C and consists of only two data points. Both the susceptibility curves and pTRM checks show alteration in this temperature range so using the whole temperature range is not reliable for paleointensity determination.

This effect is also seen for sites MT and NA. These sites yield values comparable to the present day intensity, so there is no reason to expect that the sites IN2 and OI yielded large overestimates. Sites AG and MC do no show this effect, but are not heated to 600 °C. Site MC cannot be compared to values obtained from other methods, but site AG yields most consistent paleointensities among the different methods. We expect the paleointensities obtained by the Thellier method to be an upper bound and the actual paleointensity to be between these values and those that are obtained by the other two methods.

5.3.2. Multispecimen method

To prevent any (chemical) alteration or magnetic history effects, specimens are heated only once in the MSP-DB protocol (Dekkers and Böhnel, 2006). The phenomenological model of Fabian and Leonhardt (2010) describes that PSD grains yield overestimates and they introduced the MSP-DSC protocol to correct for this magnetic tail and domain state effects. However, in recent studies (De Groot, Dekkers, et al., 2012; de Groot et al., under revision) both MSP protocols were applied to historical lavas of Mt. Etna and underestimates were found. Even the MSP-DB protocol yielded underestimates, despite the fact that all sites showed PSD behavior.

De Groot, Dekkers, et al., (2012) showed that the ARM-test was capable to qualitatively differentiate between good estimates and under- or overestimates. All sites of group I passed the ARM-test, so no underestimates are expected for those sites. Site IN1 is the only site that might yield an underestimate. It acquires more ARM after heating and is therefore expected to acquire more pTRM in the MSP experiments, leading to an underestimate of the paleofield.

Despite the fact that rock-magnetic analyses and ARM-tests did not give rise to any form of altera-

tion for samples of group I, the relative alteration error ε_{alt} was assessed for all sites that were subjected to the MSP method (Fabian and Leonhardt, 2010). This parameter yielded rather high values of 2 - 14%, whereas maximally 3% is preferred. Although not indicated by any of the preliminary measurements, specimens are obviously subject to alteration. Furthermore, we compared the difference between m_4 and m_1 to the part that is demagnetized, $m_0 - (m_1 + m_2) / 2$, and to the part that is remagnetized, $(m_1 - m_2) / 2$. Depending on the site and the applied field strength, alteration then varies between 10 and even 120%. This means that the alteration is always significant and in some cases can be as large as the (de)magnetized part in one of the MSP steps.

Although this relative alterations might not assert anything about the first step of the MSP method, which is used for the MSP-DB protocol, it does clarify that the specimens are altered during subsequent heatings. It seems that a progressive alteration occurs because of the difference between two similar magnetization steps. A single alteration that remains constant can be ruled out as it would be imparted in the first magnetization step m_1. Therefore, especially the corrections that are applied in the MSP-DSC method, which depend on m_1, m_2, and m_3, are questionable.

When not only the absolute value is assessed, it is shown that m_4 is always smaller than m_1, indicating that after several heatings to the same temperature specimens are less able to acquire a magnetization. It is plausible to think that also m_2 and m_3 would acquire a lower magnetization than would it have been the first step of the protocol. A lower m_2 and m_3 would lead to a larger Q_{DSC} (equation 3.6), thereby decreasing the obtained paleointensity. This could explain the (too) strong downward correction that is applied by the MSP-DSC protocol.

Overprints can be another reason to doubt the outcome of the MSP experiments. Samples with clear overprints can be rejected beforehand by assessing the Zijderveld diagrams, but they can also be identified during the MSP experiments. As the specimens are aligned with their original NRM during all heatings, the resulting magnetization should also have the same orientation. A deviation of > 5° compared to the orientation of the NRM is suspect. For sites of group I this rarely occurs, mostly in the case of m_2 when a large part of the NRM is removed and an opposite magnetization is applied that results in a small remanent magnetization.

For sites CS and IN1, however, all specimens show a deviation > 5° for one or more of the four measurements. From the NRM decay curves and the Zijderveld diagram of site CS it can be seen that the overprint is just removed at the set temperature of 240 °C. Comparing the remagnetization steps of the MSP protocol to the original NRM does not tell anything about the paleointensity that is pursued, which can explain the rather high paleointensity that results from the MPS experiments. For site IN1 an overprint is also clear, although less pronounced. Another feature is important here, as quite a large fraction of the NRM is removed at the set temperature which leads to negative magnetizations for m_2 at higher field strengths that must be corrected for.

Because of the overprints of sites CS and IN1 resulting paleointensities are not reliable. Furthermore, alteration can be seen in all specimens. Therefore, paleointensities are too strongly corrected in the MSP-DSC protocol, leading to underestimates. In the MSP-DB method, as in the ARM-test, samples are heated only once and alteration should not play that large a role. Since all sites of group I pass the ARM-test, we assume the paleointensities that are obtained with the MSP-DB method to be reliable. Results are lower than those from the Thellier method, being a lower bound for the actual paleointensity.

Possible explanations for underestimates, even with the MSP-DB method, were assessed by de

Site	Age (ka)	σ (ka)	MSP-DB PI (μT)	Thellier PI (μT)
AG	154.9	8.5	33.3	34.8
IN2	-	-	43.8	76.3
MT	126.4	2.4	34.4	48.0
NA	111.9	4.6	30.9	40.5
OI	28.6	4.7	66.5	122.3

Table 5.1. Summary of the technically good paleointensity results that are obtained from the MSP-DB and Thellier-Thellier method, which are used as a lower and upper bound respectively.

Groot et al. (under revision). As is the case in this study, rock-magnetic analyses and ARM-tests are used to anticipate any chemical or magnetic alteration. Although not tested in this study, the cooling rate is also ruled out as a significant effect as a more natural slower cooling rate only enlarges the underestimate. Subtle changes that occur in the ARM-test can only have a magnetic cause (De Groot, Dekkers, et al., 2012): a possible explanation might be transdomain transitions of metastable domain states. This would cause specimens to acquire more magnetization after heating, leading to an underestimate of the paleointensity. However, this would still not explain the decreasing acquisition of magnetization after several heatings and the higher paleointensities that are obtained in the Thellier experiments since it is expected that specimens would acquire more magnetization in certain temperature ranges and yield underestimates as well.

5.3.3. Pseudo-Thellier method

As explained before, the pseudo-Thellier method is a relative method to obtain the paleointensity. Relative pTh-slopes are related to absolute values by De Groot, Biggin, et al. (2012) with a calibration formula that is gauged on historical lavas from Hawaii. The use of this formula leads to rather low paleointensities compared to the other methods that were used in this study. However, this formula is not tested on historical lavas from Mt. Etna with known reference values. A difference in rock-magnetic properties probably causes the calibration formula not to be applicable to the samples in this study.

Although specimens yielding low (high) paleointensities with the two absolute methods generally also yield low (high) pTh-slopes, a linear correlation cannot easily be obtained with either one of the absolute methods. For example, sites IN2 and OI yield similar pTh-slopes but site OI yield roughly 50% higher absolute paleointensities. Still too little is known about this new method to make any conclusive remarks about it.

5.3.4. Comparison

The outcomes of the different paleointensity methods per site vary. The pseudo-Thellier method always yields the lowest paleointensity but the absolute values are discarded because we think the calibration formula gauged on historical lavas from Hawaii is not applicable for these lavas from Mt. Etna. Results from the MSP-DSC method are also discarded because of alteration that occurs in the correction steps of the protocol.

Both the Thellier method and the MSP-DB method produce technically good results so there is no reason to reject these results. The Thellier method consistently yields higher values, which we will take as an upper bound. Paleointensities that are obtained by the MSP-DB protocol are always lower, although varying in absolute and relative difference, and are taken as a lower bound (table 5.1, figure 5.1).

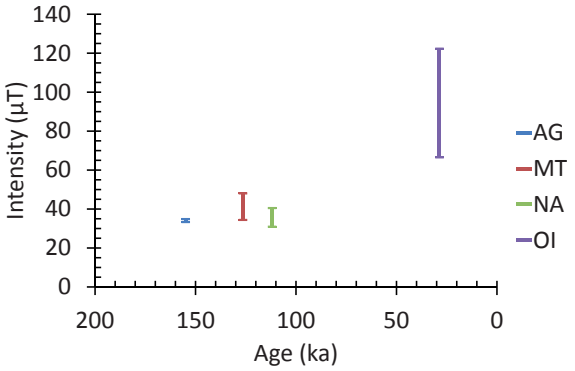

Fig. 5.1. Plot of the technically good paleointensity results versus age. The MSP-DB results are used as a lower bound, the Thellier-Thellier results as an upper bound. Site IN2 could not be plotted because the age is unknown.

Only sites from group I produced paleointensities with both methods. Only for site AG results overlap within the uncertainty, which results in a range of 33.3 - 34.8 µT. The difference for sites MT (34.4 - 48.0 µT) and NA (30.9 - 40.5 µT) is quite small and the paleointensities are closest to the current intensity of 45.0 µT. The range of paleointensities is larger for the two remaining sites, IN2 and OI. Site IN2 yields a paleointensity that is at the upper limit of the present day value: 43.8 - 76.3 µT. Site OI clearly stands out with an estimated paleointensity of 66.5 - 122.3 µT.

6. Conclusion

The technically acceptable outcomes of the different paleointensity methods used in this study do not agree mutually. However, a clear trend can be seen between the methods. Pseudo-Thellier yields the lowest values but the calibration formula that is used to relate pTh-slopes to absolute paleointensities might not be applicable to lavas from Mt. Etna due to differences in rock-magnetic properties. No clear (linear) trend can be found to relate the pTh-factors to one of the absolute methods because of the limited data available.

The MSP-DSC method yields slightly higher values, but this method has shown to produce underestimates for some historical lavas from Mt. Etna. Although not shown by the preliminary measurements, subtle alteration can explain the (too) large negative corrections of the MSP-DSC protocol. The MSP-DB protocol has also shown to produce underestimates on historical lavas. However, our lavas pass the ARM-tests which indicates that the results reproduce the paleointensity more reliably. Alteration caused by transdomain transitions of metastable domain states can however still play a role and explain underestimates. The Thellier method produces rather high paleointensities. These might be too high as only a relatively small fraction of the NRM is unblocked at high temperatures.

The actual intensities of the paleofield most probably are in the range between those obtained by the Thellier and MSP-DB method. It is hard to estimate which of the two is most reliable, as both yield technically good results and have produced variable results on historical samples that could be related to IGRF values. From the resulting paleointensities it is observed that none of the evaluated sites show the low values up to 20 μT that are related to an excursion. The values are in a range of 30.9 - 122.3 μT and most results are comparable in magnitude to the present day intensity of 45.0 μT.

Based on the directional behavior, some sites might suggest an excursion. Two sites are in the right age interval for the Laschamp excursion and show directions that could be related to a transitional VGP. Two more sites with directions of the VGP somewhat deviating from the true north have an age slightly older than the Blake excursion. Except for one site, however, these sites could not produce a paleointensity to assert this assumption.

Acknowledgements

I am very grateful for the help I received during my Master's research project at Paleomagnetic Laboratory 'Fort Hoofddijk'. In particular I would like to thank Lennart de Groot, my supervisor, for his willingness to help, his answers to my questions, and his critical notes during this study. I am grateful to prof. dr. Cor Langereis and dr. Mark Dekkers for finding me this research project including the fieldwork to Mount Etna and to Marilyn Monster for collaboration in the lab and in the field. The help of Tom Mullender and Maxim Krasnoperov with regard to the laboratory equipment is very much appreciated. Besides Lennart de Groot, I would like to thank dr. Klaudia Kuiper of VU University Amsterdam for supervising in the field. Finally, I am very grateful to dr. Stefano Branca of the (Italian) National Institute of Geophysics and Volcanology, section Catania, for his help and experience in the field on Mount Etna.

References

Aitken, M., Allsop, A., Bussell, G., Winter, M., 1988. Determination of the intensity of the Earth's magnetic field during archaeological times: reliability of the Thellier technique. Reviews of Geophysics 26, 3–12.

Biggin, A.J., Perrin, M., Dekkers, M.J., 2007. A reliable absolute palaeointensity determination obtained from a non-ideal recorder. Earth and Planetary Science Letters 257, 545–563.

Biggin, A.J., Poidras, T., 2006. First-order symmetry of weak-field partial thermoremanence in multi-domain ferromagnetic grains. 1. Experimental evidence and physical implications. Earth and Planetary Science Letters 245, 438–453.

Branca, S., Coltelli, M., Gropelli, G., Lentini, F., 2011. Geological map of Etna volcano, 1: 50,000 scale. Italian Journal of Geosciences 130, 265–291.

Chauvin, A., Duncan, R., Bonhommet, N., Levi, S., 1989. Paleointensity of the Earth's magnetic field and K-Ar dating of the Louchadiere volcanic flow (Central France): new evidence for the Laschamp excursion. Geophysical Research Letters 16, 1189–1192.

Coe, R., Grommé, S., Mankinen, E., 1978. Geomagnetic paleointensities from radiocarbon-dated lava flows on Hawaii and the question of the Pacific nondipole low. Journal of Geophysical Research 83, 1740–1756.

Coe, R.S., 1967. The determination of paleo-intensities of the Earth's magnetic field with emphasis on mechanisms which could cause non-ideal behavior in Thellier's method. Journal of Geomagnetism and Geoelectricity 19, 157–178.

Day, R., Fuller, M., Schmidt, V., 1977. Hysteresis properties of titanomagnetites: grain-size and compositional dependence. Physics of the Earth and Planetary Interiors 13, 260–267.

De Beni, E., Branca, S., Coltelli, M., Gropelli, G., Wijbrans, J.R., 2011. 40Ar/39Ar isotopic dating of Etna volcanic succession. Italian Journal of … 130, 292–305.

De Groot, L. V., Biggin, A.J., Dekkers, M.J., Herrero-Bervera, E., 2012. A new 2000 year record of geomagnetic intensity variations from Hawaii. GP43A-1122.

De Groot, L. V., Dekkers, M.J., Mullender, T.A.T., 2012. Exploring the potential of acquisition curves of the anhysteretic remanent magnetization as a tool to detect subtle magnetic alteration induced by heating. Physics of the Earth and Planetary Interiors 194-195, 71–84.

De Groot, L. V., Mullender, T.A.T., Dekkers, M.J., under revision. An evaluation of the influence of the experimental cooling rate along with other thermomagnetic effects to explain anomalously low paleointensities obtained for historic lavas of Mt. Etna (Italy).

Dekkers, M.J., Böhnel, H.N., 2006. Reliable absolute palaeointensities independent of magnetic domain state. Earth and Planetary Science Letters 248, 508–517.

Del Carlo, P., Branca, S., De Beni, E., Lo Castro, M.D., Wijbrans, J.R., 2012. The Mt. Moio eruption (Etna): Stratigraphy, petrochemistry and 40Ar/39Ar age determination with inferences on the relationship between structural setting and magma intrusion. Journal of Volcanology and Geothermal Research 241-242, 49–60.

Driscoll, P., Olson, P., 2009. Polarity reversals in geodynamo models with core evolution. Earth and Planetary Science Letters 282, 24–33.

Dunlop, D.J., 2011. Physical basis of the Thellier–Thellier and related paleointensity methods. Physics of the Earth and Planetary Interiors 187, 118–138.

Dunlop, D.J., Özdemir, Ö., 1997. Rock Magnetism: Fundamentals and Frontiers. Cambridge University Press.

Fabian, K., Leonhardt, R., 2010. Multiple-specimen absolute paleointensity determination: An optimal protocol including pTRM normalization, domain-state correction, and alteration test. Earth and Planetary Science Letters 297, 84–94.

Fang, X.-M., Li, J.-J., Van der Voo, R., Mac Niocaill, C., Dai, X.-R., Kemp, R. a., Derbyshire, E., Cao, J.-X., Wang, J.-M., Wang, G., 1997. A record of the Blake Event during the last interglacial paleosol in the western Loess Plateau of China. Earth and Planetary Science Letters 146, 73–82.

Ferk, A., Leonhardt, R., 2009. The Laschamp geomagnetic field excursion recorded in Icelandic lavas. Physics of the Earth and Planetary Interiors 177, 19–30.

Griffiths, D.J., 1999. Introduction to Electrodynamics. Prentice Hall.

Gubbins, D., 1999. The distinction between geomagnetic excursions and reversals. Geophysical Journal International 137, F1–F4.

Guillou, H., Singer, B.S., Laj, C., Kissel, C., Scaillet, S., Jicha, B.R., 2004. On the age of the Laschamp geomagnetic excursion. Earth and Planetary Science Letters 227, 331–343.

Hollerbach, R., Jones, C., 1993. Influence of the Earth's inner core on geomagnetic fluctuations and reversals. Nature 365, 541–543.

Kissel, C., Laj, C., 2004. Improvements in procedure and paleointensity selection criteria (PICRIT-03) for Thellier and Thellier determinations: application to Hawaiian basaltic long cores. Physics of the Earth and Planetary Interiors 147, 155–169.

Leonhardt, R., Heunemann, C., Krása, D., 2004. Analyzing absolute paleointensity determinations: Acceptance criteria and the software ThellierTool4.0. Geochemistry Geophysics Geosystems 5, Q12016.

Meynadier, L., Valet, J.-P., Weeks, R., Shackleton, N.J., Hagee, V.L., 1992. Relative geomagnetic intensity of the field during the last 140 ka. Earth and Planetary Science Letters 114, 39–57.

Riisager, P., Riisager, J., 2001. Detecting multidomain magnetic grains in Thellier palaeointensity experiments. Physics of the Earth and Planetary Interiors 125, 111–117.

Roperch, P., Bonhommet, N., Levi, S., 1988. Paleointensity of the earth's magnetic field during the Laschamp excursion and its geomagnetic implications. Earth and Planetary Science Letters 88, 209–219.

Selkin, P.A., Tauxe, L., 2000. Long-term variations in palaeointensity. Philosophical Transactions of the Royal Society A: Mathematical, Physical and Engineering Sciences 358, 1065–1088.

Shaw, J., 1974. A new method of determining the magnitude of the palaeomagnetic field: application to five historic lavas and five archaeological samples. Geophysical Journal of the Royal Astronomical Society 39, 133–141.

Singer, B.S., Guillou, H., Jicha, B.R., Laj, C., Kissel, C., Beard, B.L., Johnson, C.M., 2009. 40Ar/39Ar, K–Ar and 230Th–238U dating of the Laschamp excursion: A radioisotopic tie-point for ice core and climate chronologies. Earth and Planetary Science Letters 286, 80–88.

Tauxe, L., 2010. Essentials of Paleomagnetism. University of California Press.

Tauxe, L., Pick, T., Kok, Y., 1995. Relative paleointensity in sediments: a pseudo-Thellier approach. Geophysical Research Letters 22, 2885–2888.

Tauxe, L., Staudigel, H., 2004. Strength of the geomagnetic field in the Cretaceous Normal Superchron: New data from submarine basaltic glass of the Troodos Ophiolite. Geochemistry Geophysics Geosystems 5, Q02H06.

Thellier, E., Thellier, O., 1959. Sur l'intensité du champ magnétique terrestre dans le passé historique et géologique. Annales de Geophysique.

Tric, E., Laj, C., Valet, J.-P., Tucholka, P., Paterne, M., Guichard, F., 1991. The Blake geomagnetic event: transition geometry, dynamical characteristics and geomagnetic significance. Earth and Planetary Science Letters 102, 1–13.

Valet, J.-P., 2003. Time variations in geomagnetic intensity. Reviews of Geophysics 41, 1004.

Vandamme, D., 1994. A new method to determine paleosecular variation. Physics of the Earth and Planetary Interiors 85, 131–142.

Vérard, C., Leonhardt, R., Winklhofer, M., Fabian, K., 2012. Variations of magnetic properties in thin lava flow profiles: Implications for the recording of the Laschamp Excursion. Physics of the Earth and Planetary Interiors 200-201, 10–27.

Yu, Y., Dunlop, D.J., Özdemir, Ö., 2003. Are ARM and TRM analogs? Thellier analysis of ARM and pseudo-Thellier analysis of TRM. Earth and Planetary Science Letters 205, 325–336.

Yu, Y., Tauxe, L., Genevey, A., 2004. Toward an optimal geomagnetic field intensity determination technique. Geochemistry Geophysics Geosystems 5, Q02H07.

APPENDICES

A.1. Magnetic susceptiblity and NRM decay curves

AG

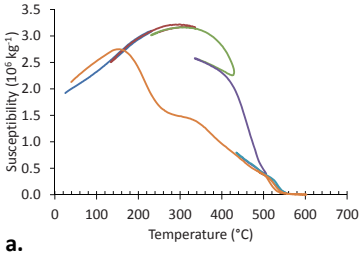

1. a.

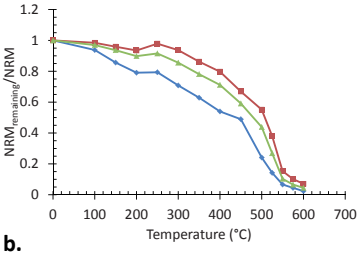

b.

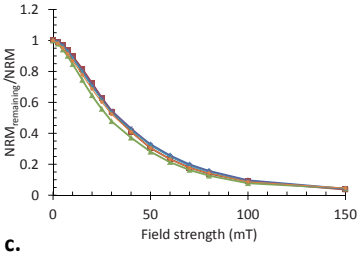

c.

BT

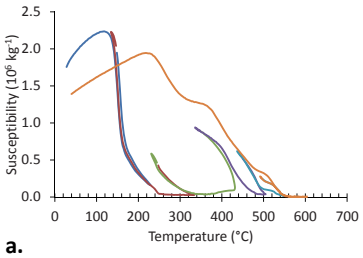

2. a.

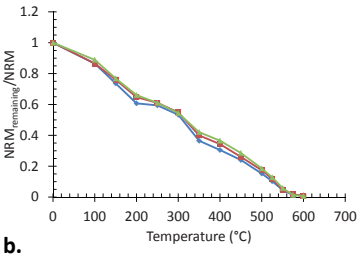

b.

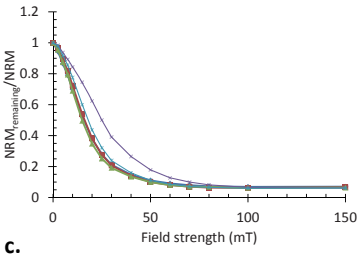

c.

CS

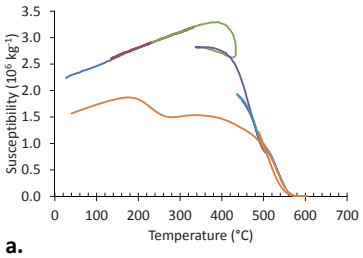

3. a.

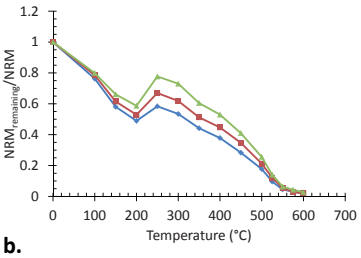

b.

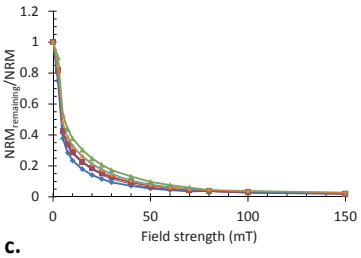

c.

DM1

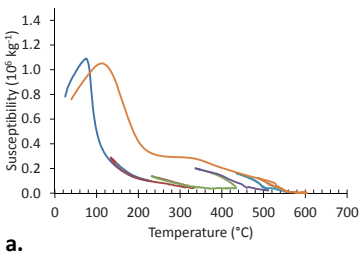

4. a.

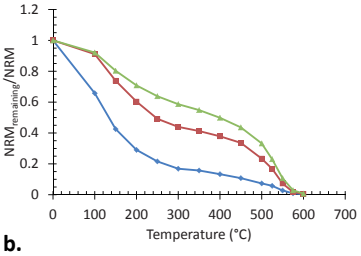

b.

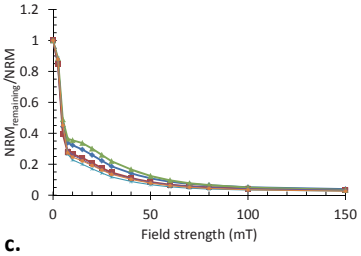

c.

DM2

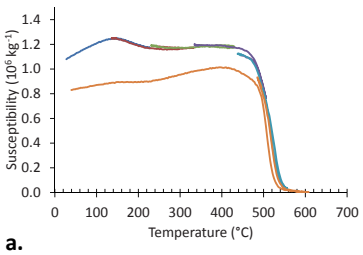

5. a.

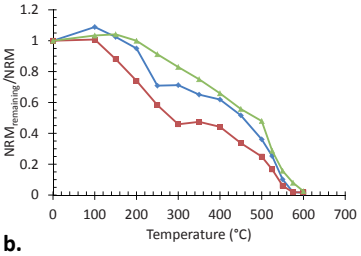

b.

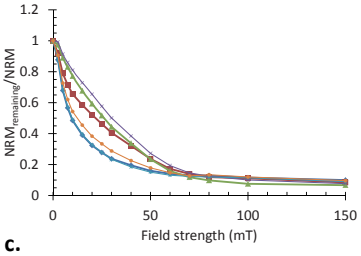

c.

IN1

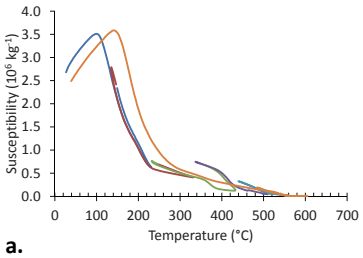

6. a.

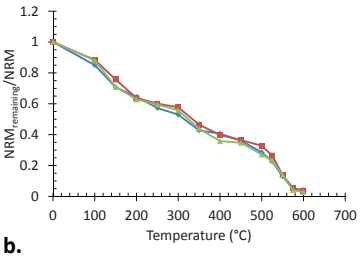

b.

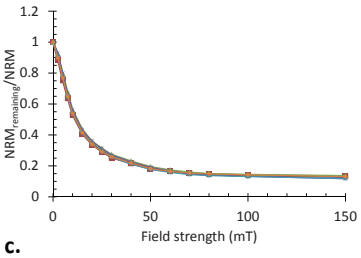

c.

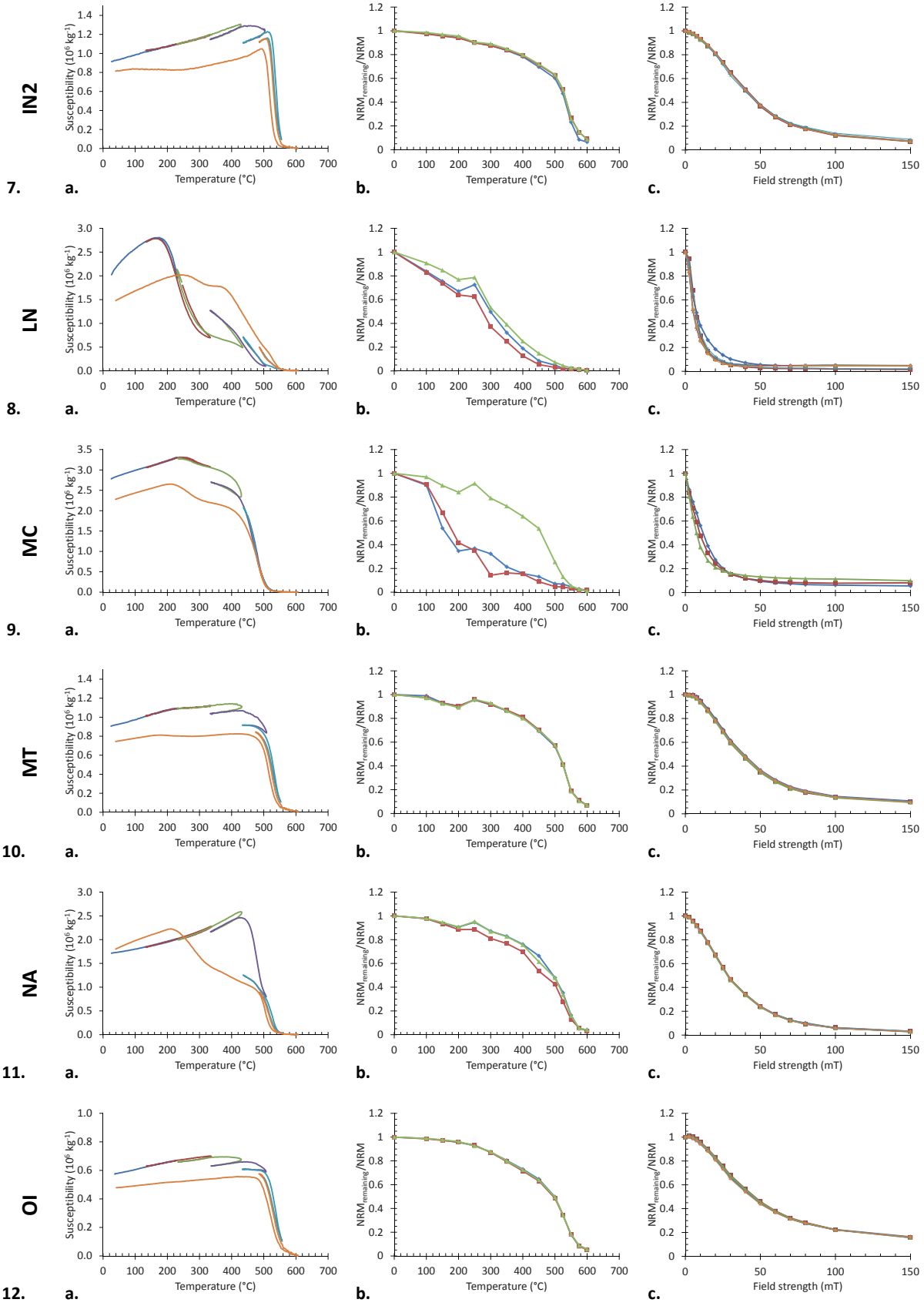

Fig. A1.1-15. Magnetic susceptibility versus temperature (**a.**) and both thermal (**b.**) and AF (**c.**) NRM decay curves for all sites. Continued on next page.

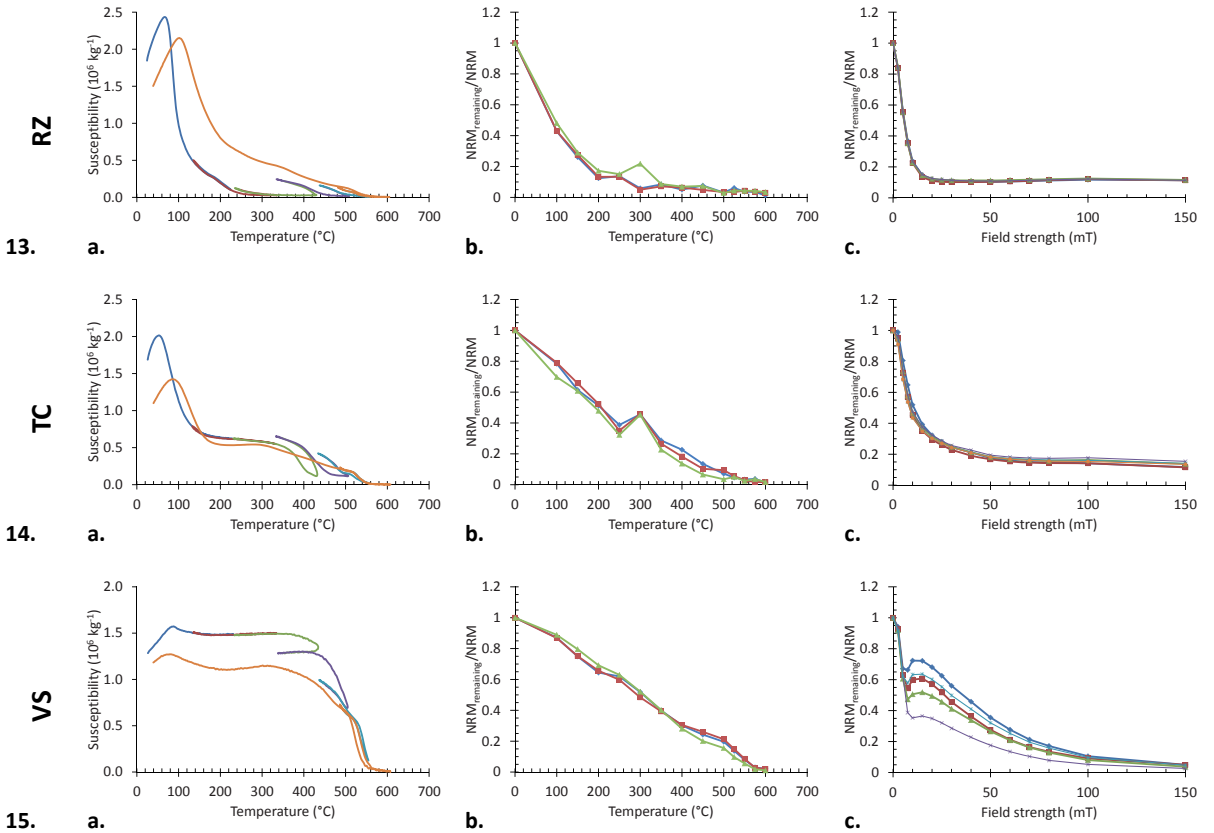

Fig. A1.1-15. Magnetic susceptibility versus temperature (**a.**) and both thermal (**b.**) and AF (**c.**) NRM decay curves for all sites. Based on the magnetic susceptibility curves, a categorization is made into groups L (sites BT, DM1, and RZ), M (sites IN1, LN, and TC), and H (sites AG, CS, DM2, IN2, MC, MT, NA, OI, and VS). Group L loses > 80% of its maximal suceptibilty at 200 ° C, group H loses < 20% at 400 °C, and group M is an intermediate group with possibly multiple Curie temperatures. Alteration temperatures and Curie temperatures are given in table 4.1. This behavior is reflected in the thermal NRM decay curves, as sites of group L and M generally lose their magnetization at lower temperatures than sites of group H. Sites of group I (AG, IN2, MT, NA, and OI; see text) lose very little magnetization up to high temperatures, resulting in convex-shaped curves. These sites also get AF demagnetized less easy and can hold up to 15% of the original NRM at 150 mT.

A.2. Zijderveld diagrams

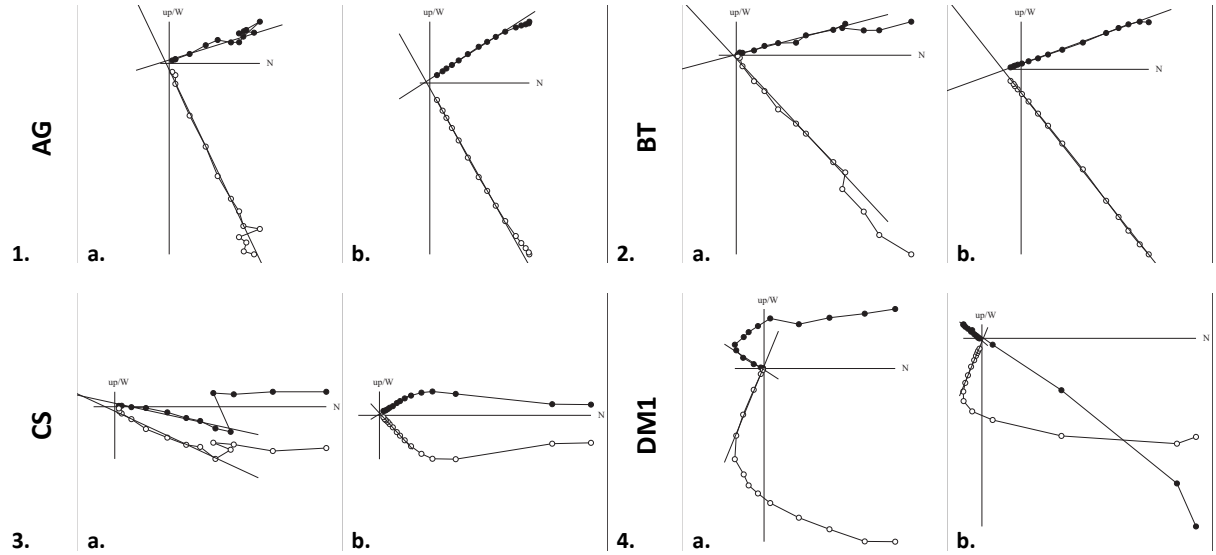

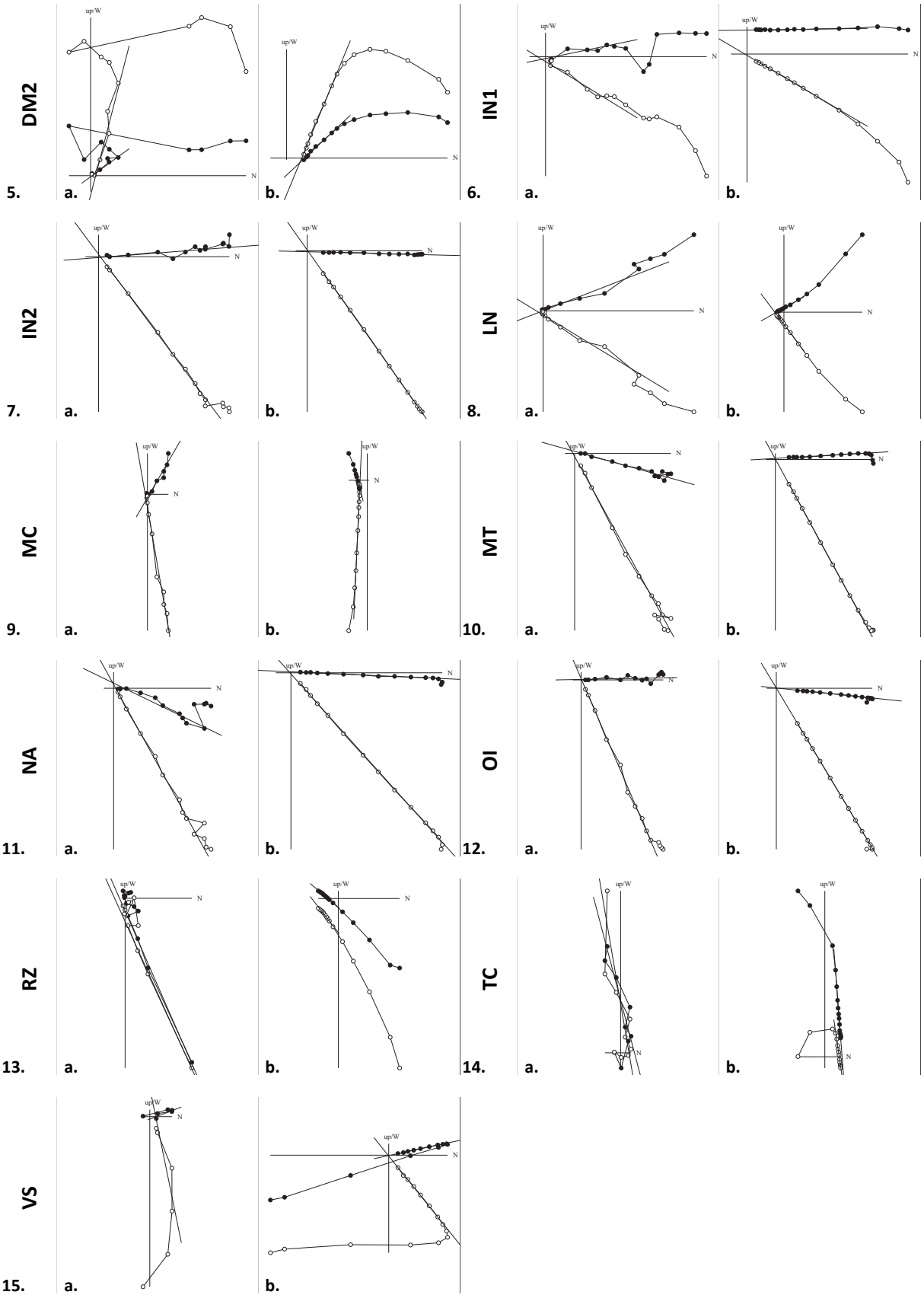

Fig. A2.1-15. Zijderveld diagrams for thermal (**a.**) and AF (**b.**) demagnetization. Generally directions agree between both diagrams. Best diagrams are obtained for sites of group I (AG, IN2, MT, NA, and OI; see text), only minor overprints occur and magnetization decays through the origin.

A.3. ARM-tests

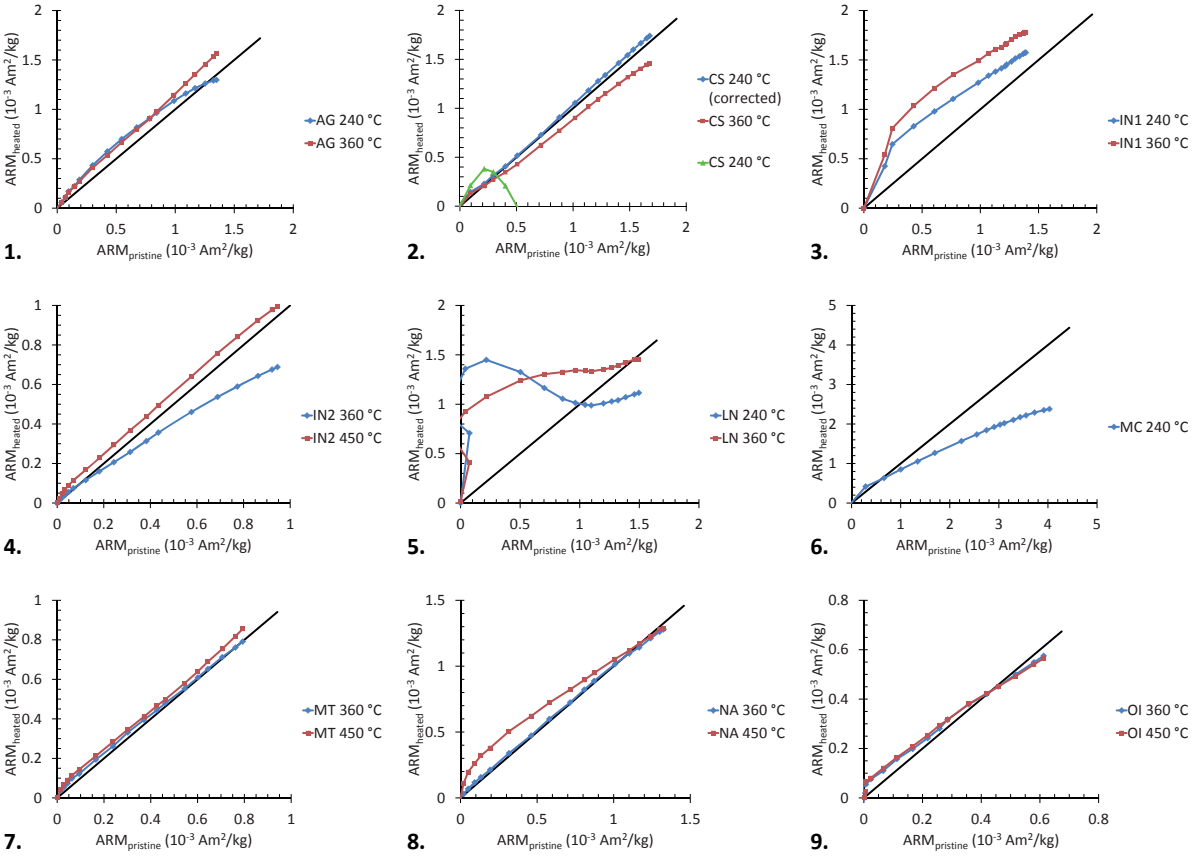

Fig. A3.1-9. ARM-tests for the subset of sites that were selected based on the rock-magnetic analyses and demagnetization. Except for site MC, all sites were tested at two temperatures. The data of site CS at 240 °C were corrected (see text). Sites LN and MC were discarded for the MSP experiments. For all the other sites, the lowest temperature was chosen as set temperature in the MSP experiments, as data generally shows more desirable behavior close to the diagonal.

A.4. Thellier-Thellier diagrams

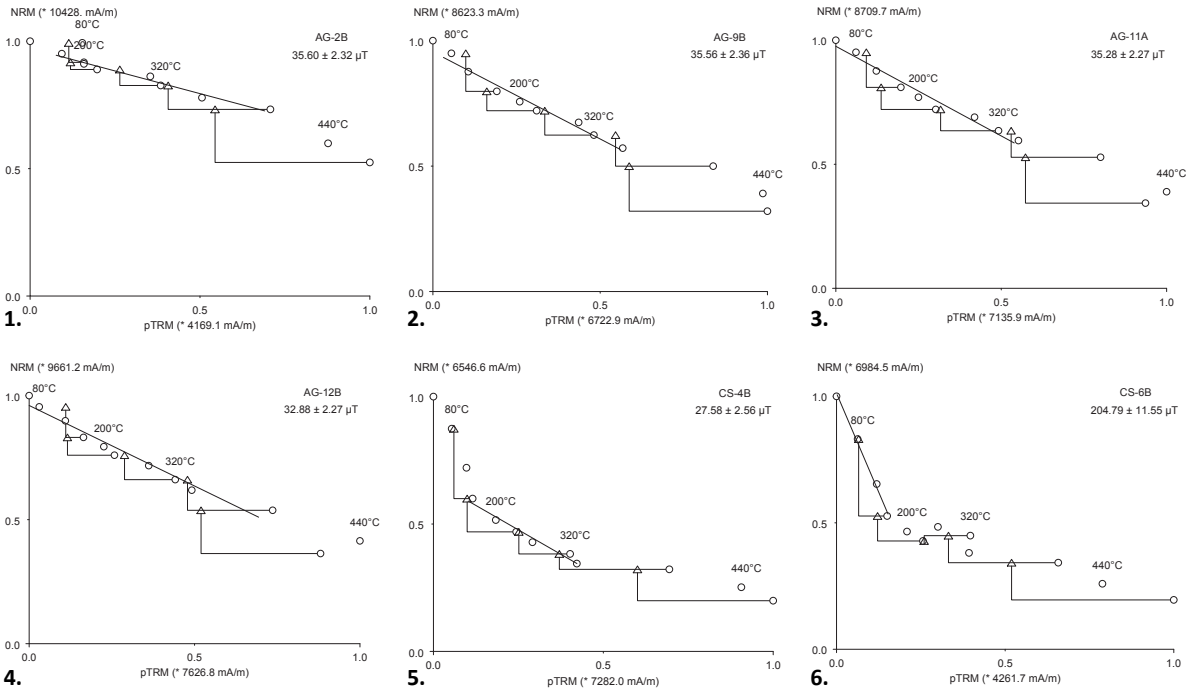

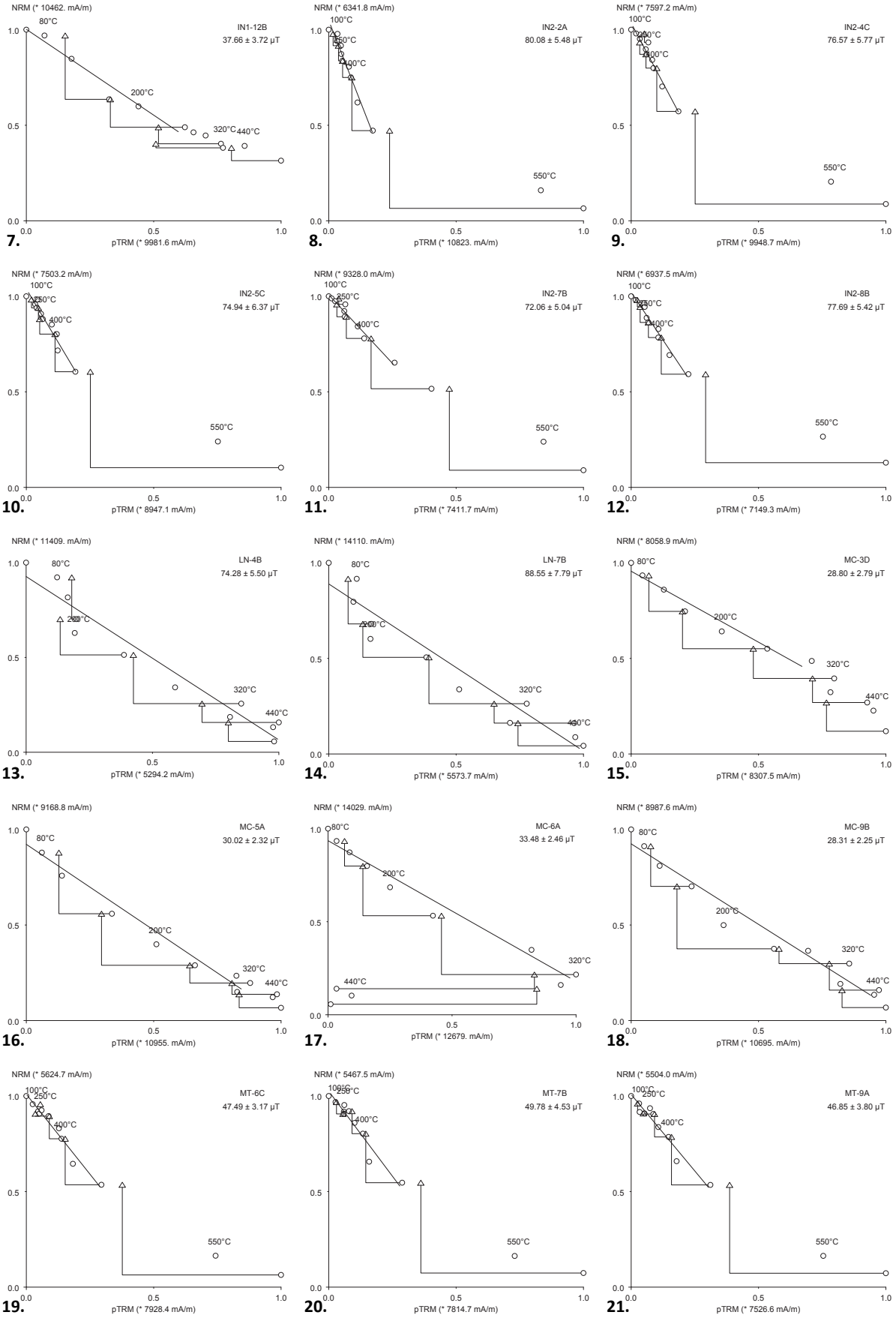

Fig. A4.1-33. Thellier-Thellier Arai diagrams for all specimens that passed one of the sets of selection criteria (see text). Continued on next page.

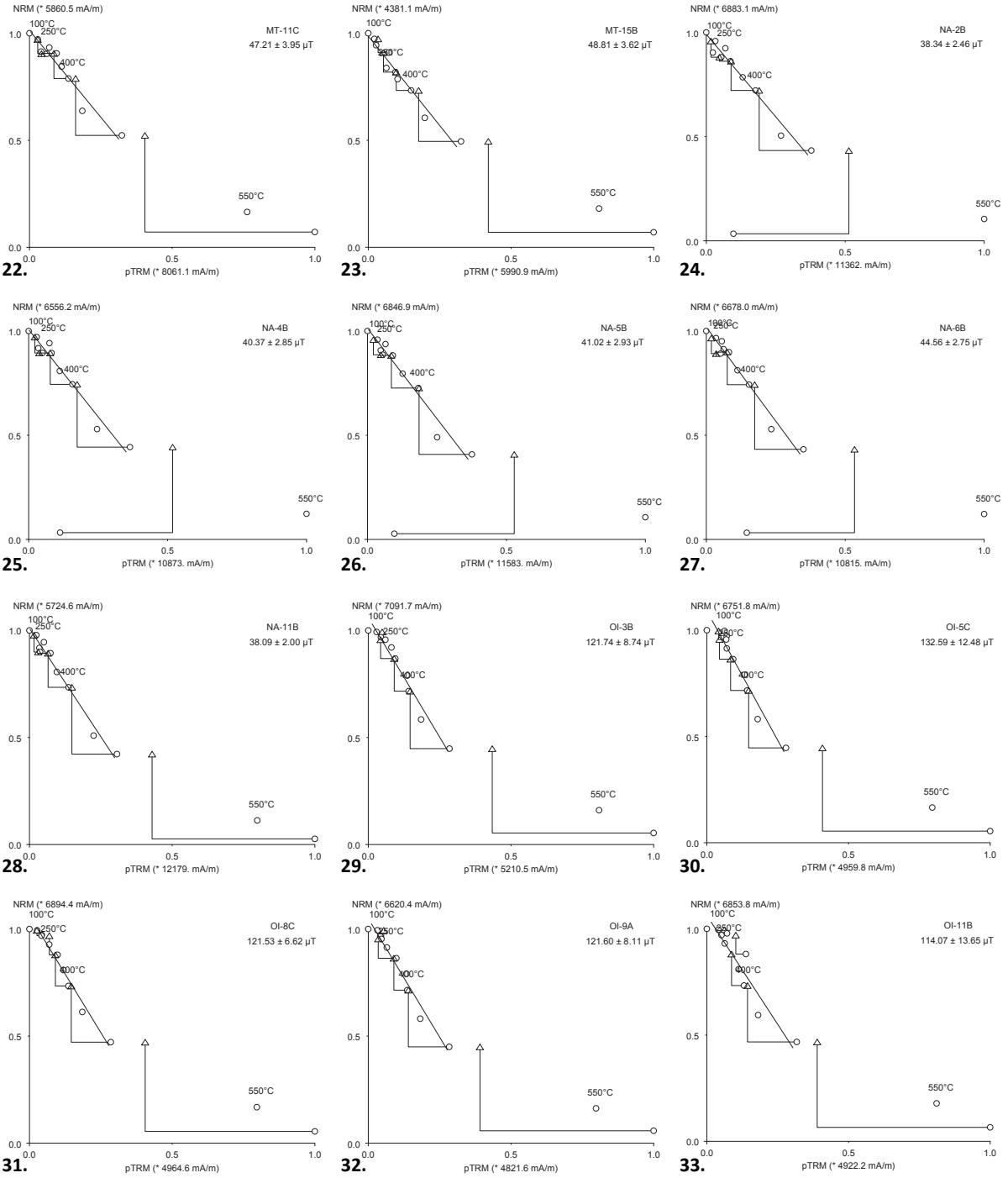

Fig. A4.1-33. Thellier-Thellier Arai diagrams for all specimens that passed one of the sets of selection criteria (see text). Although passing the criteria, results of site CS (**5.** and **6.**) were discarded because two totally different temperature intervals are used for the linear fit and sagging and/or the removal of an overprint is clearly visible. Sites IN1 (**7.**) and LN (**13.** and **14.**) also show sagging and very bad pTRM checks. The results are therefore discarded. Sites AG (**1.** - **4.**) and MC (**15.** - **18.**) both show 4 specimens that passed the selection criteria, but both yield rather high values for δt*, which is reflected in moderate pTRM checks. Sites IN2 (**8.** - **12.**), MT (**19.** - **23.**), NA (**24.** - **28.**), and OI (**29.** - **33.**) show the best behavior. The paleointensity is determined over a large range of temperatures up to 500 °C and pTRM checks are generally good. Data points for temperatures > 500 °C deviate from the linear fit but have shown alteration in the susceptibility curves for this temperature. For site MT a slight zig-zag behavior is visible, which is characteristic for the effect of pTRM tails in the IZZI protocol.

A.5. Multispecimen diagrams

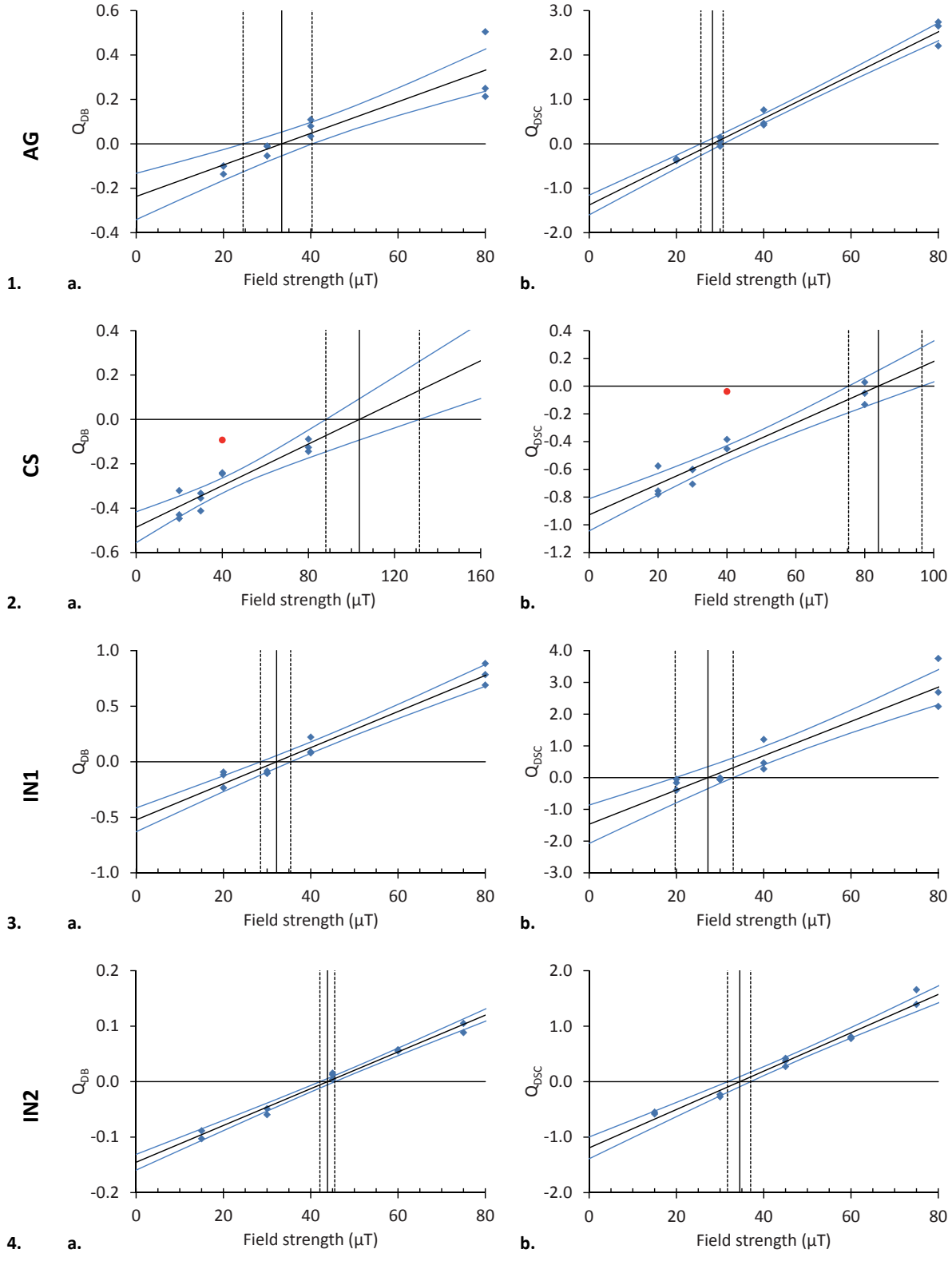

Fig. A5.1-7. MSP-DB (**a.**) and MSP-DSC (**b.**) diagrams for all sites that passed the ARM-test (see text). Continued on next page.

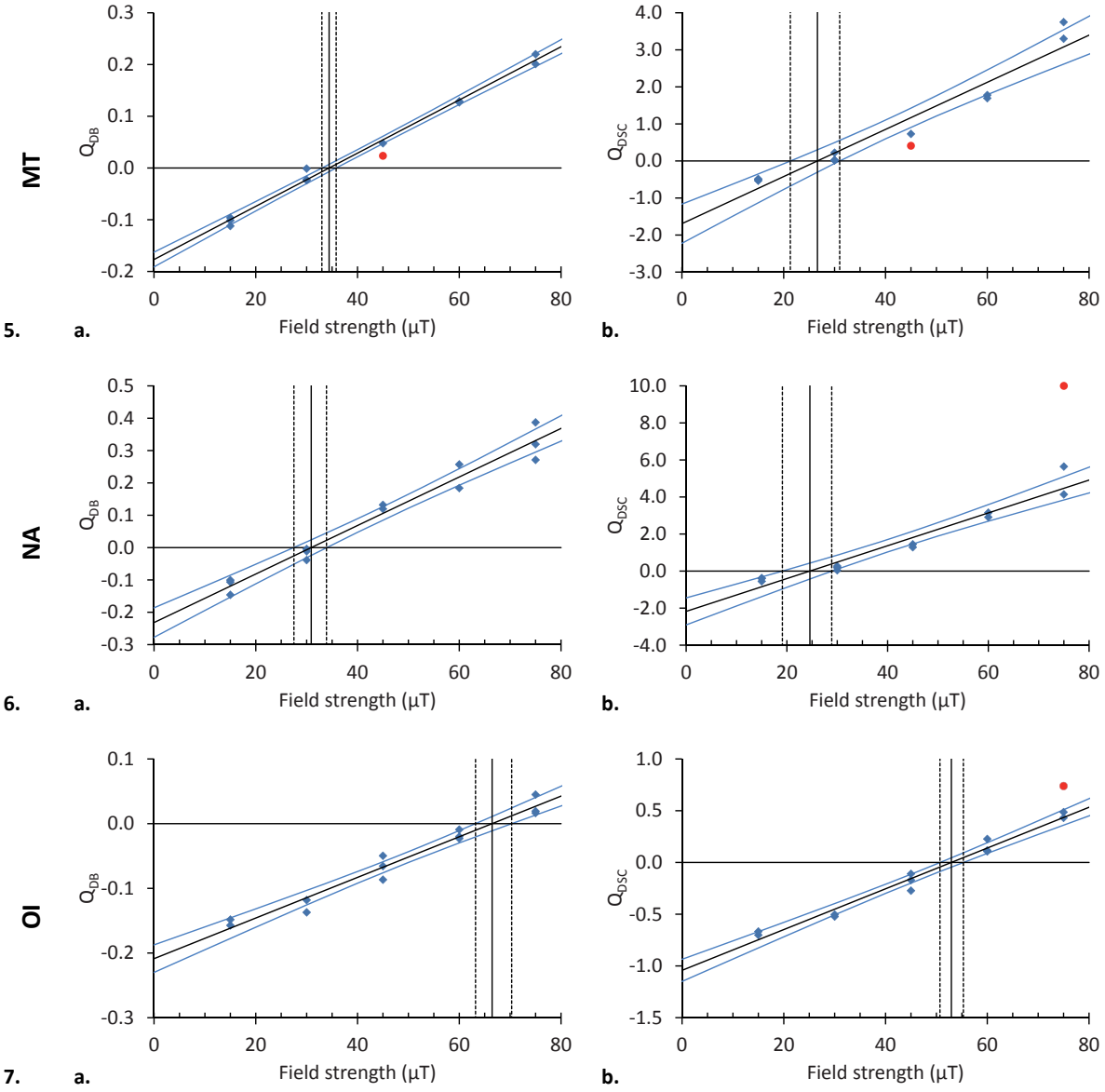

Fig. A5.1-7. MSP-DB (**a.**) and MSP-DSC (**b.**) diagrams for all sites that passed the ARM-test (see text). Data points deviating more than twice the standard deviation were omitted (red dots). For all sites the obtained paleointensity is decreased by the DSC protocol. Especially site CS yields a large confidence interval as all laboratory fields are below the estimated paleofield. Data points at 80 μT for sites AG and IN1 show some scatter and cause a large confidence interval, but do not significantly influence the obtained paleointensity. Sites IN2, MT, NA, and OI show technically the best results with small confidence intervals.

A.6. Pseudo-Thellier diagrams

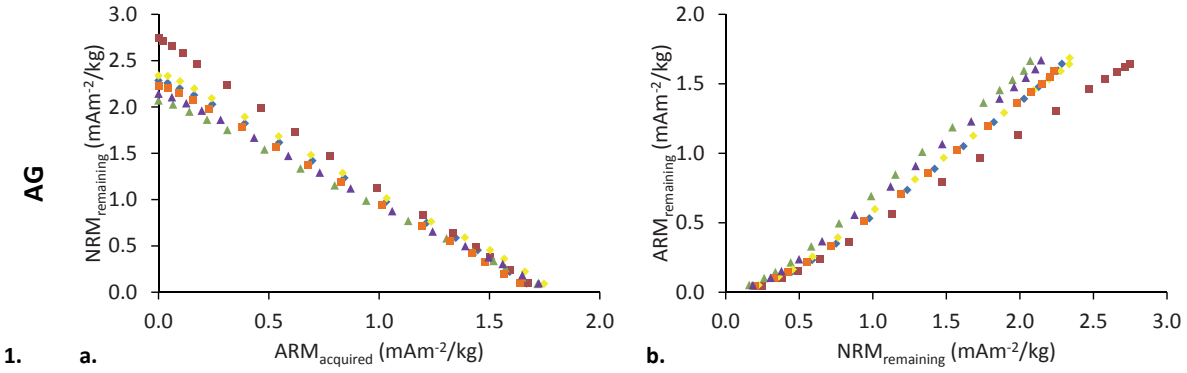

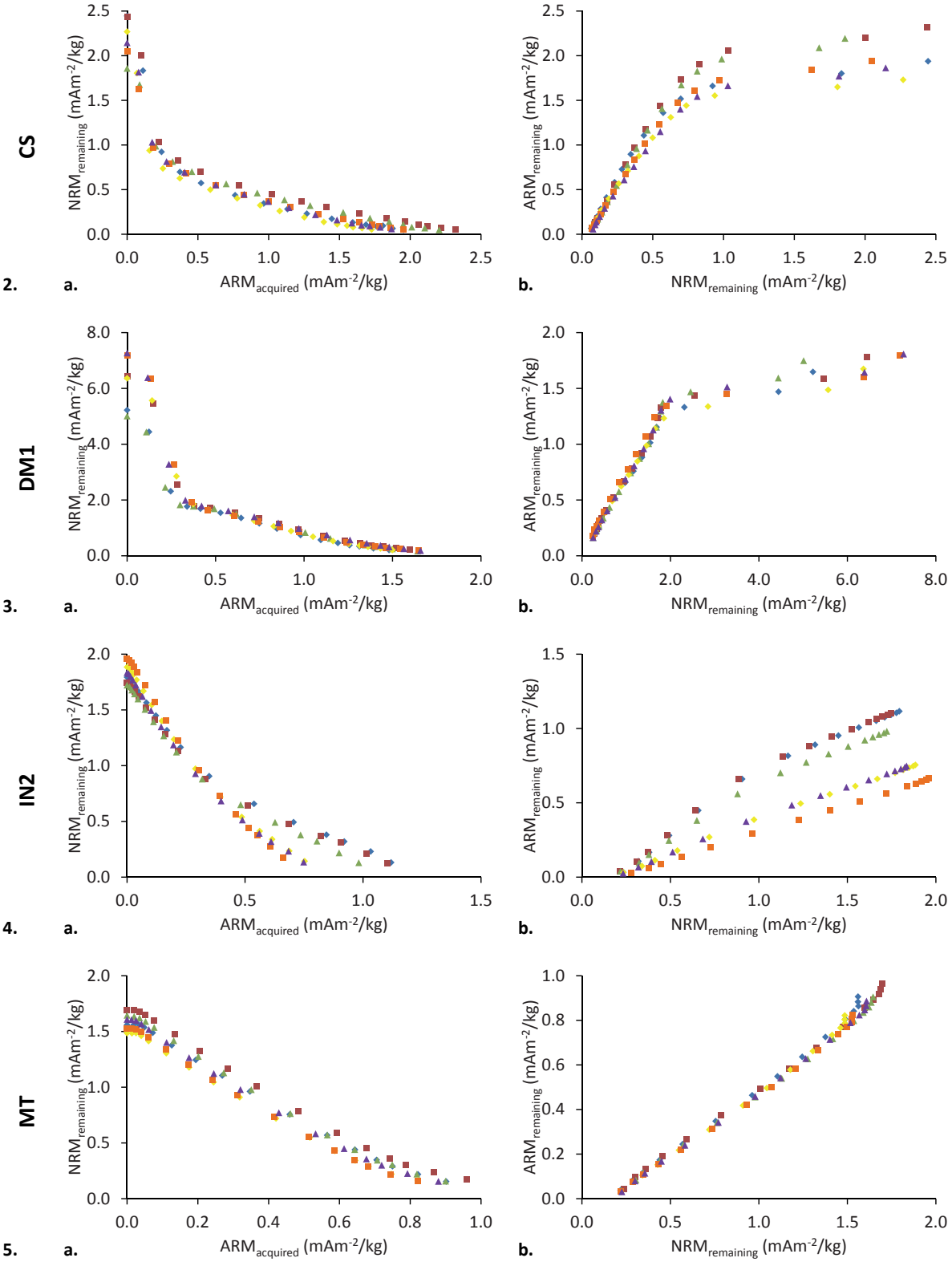

Fig. A6.1-8. ARM Arai diagrams (**a.**) and AF-ARM versus AF-NRM diagrams (**b.**) for all sites with 23 mT < $B_{1/2}$ < 63 mT (see text).
Continued on next page.

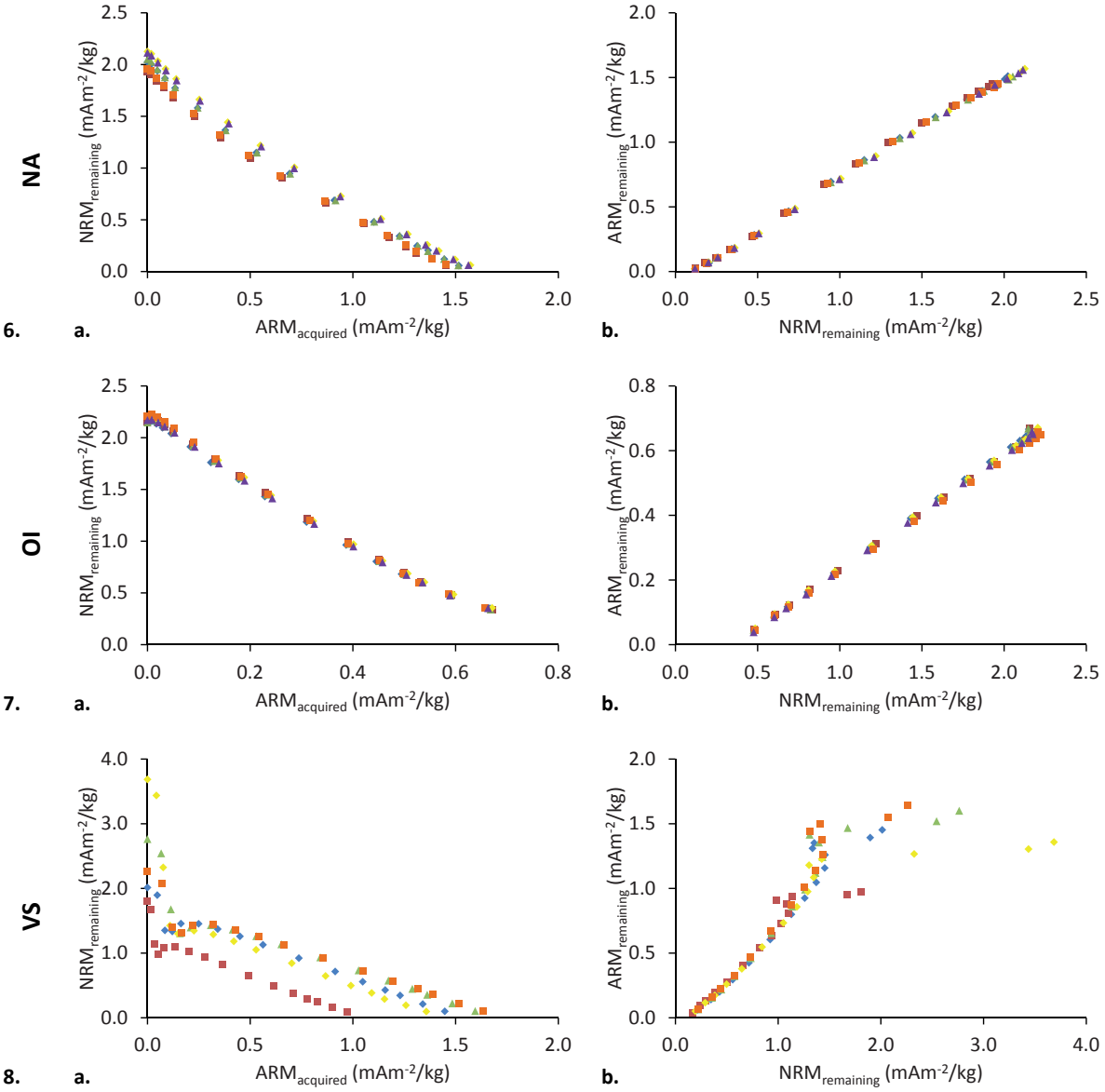

Fig. A6.1-8. ARM Arai diagrams (**a.**) and AF-ARM versus AF-NRM diagrams (**b.**) for all sites with 23 mT < $B_{1/2}$ < 63 mT (see text). The linear part of the AF-ARM versus AF-NRM diagram is selected in order to ensure that the magnetization is carried by the same magnetic grains after demagnetization. Furthermore, overprints are avoided in determining the pTh-slope in the Arai diagram. Overprints are clearly visible for sites CS, DM1, and VS, so this part is discarded. For sites AG and IN2 some variation occurs between the different specimens. Sites MT, NA, and OI show the most ideal behavior as the specimens behave very similarly and almost the full range of field strengths can be used to determine the pTh-slope.